

# Adhesion-driven patterns in a calcium-dependent model of cancer cell movement

Kaouri, K · Bitsouni, V · Buttenschön, A · Thul, R

Received: date / Accepted: date

**Abstract** Cancer cells exhibit increased motility and proliferation, which are instrumental in the formation of tumours and metastases. These pathological changes can be traced back to malfunctions of cellular signalling pathways, and calcium signalling plays a prominent role in these. We formulate a new model for cancer cell movement which for the first time explicitly accounts for the dependence of cell proliferation and cell-cell adhesion on calcium. At the heart of our work is a non-linear, integro-differential (non-local) equation for cancer cell movement, accounting for cell diffusion, advection and proliferation. We also employ an established model of cellular calcium signalling with a rich dynamical repertoire that includes experimentally observed periodic wave trains and solitary pulses. The cancer cell density exhibits travelling fronts and complex spatial patterns arising from an adhesion-driven instability (ADI). We show how the different calcium signals and variations in the strengths of cell-cell attraction and repulsion shape the emergent cellular aggregation patterns, which are a key component of the metastatic process. Performing a linear stability analysis, we identify parameter regions corresponding to ADI. These regions are confirmed by numerical simulations, which also reveal different types of aggregation patterns and these patterns are significantly affected by  $\text{Ca}^{2+}$ . Our study demonstrates that the maximal cell density decreases with calcium concentration, while the frequencies of the calcium oscillations and the cell density oscillations are approximately equal in many cases. Furthermore, as the calcium levels increase the speed of the travelling fronts increases, which is related to a higher cancer invasion potential. These novel insights provide a step forward in the design of new cancer treatments that may rely on controlling the dynamics of cellular calcium.

**Keywords** Cancer cells · Non-local model of cancer · Calcium · Cell-cell adhesion · Travelling wave · Aggregation patterns · Adhesion-driven instability · Oscillatory signalling pathway

---

K. Kaouri  
School of Mathematics, Cardiff University, CF24 4AG, UK  
Tel.: +442920875259  
E-mail: KaouriK@cardiff.ac.uk

V. Bitsouni  
SciCo Cyprus, Nicosia 1700, Cyprus & School of Mathematics, Cardiff University, CF24 4AG, UK  
E-mail: vbitsouni@gmail.com

A. Buttenschön  
Department of Mathematics, University of British Columbia, Vancouver V6T 1Z2, BC, Canada  
E-mail: abuttens@math.ubc.ca

R. Thul  
School of Mathematical Sciences & Centre for Mathematical Medicine and Biology  
University of Nottingham, Nottingham, NG7 2RD, UK  
E-mail: ruediger.thul@nottingham.ac.uk

**Mathematics Subject Classification (2000)** MSC 35B36 · MSC 35Q92 · MSC 35R09 · MSC 70K50 · MSC 92C15 · MSC 92C17 · MSC 92-08

## 1 Introduction

Cell-cell adhesion and cellular proliferation are fundamental features of multicellular organisms, along with cell division, migration and apoptosis. These processes are orchestrated and coordinated by a multitude of cellular signalling pathways (Alberts et al, 2000). When these signalling cascades are disturbed, numerous pathologies ensue, including cancer. Amongst the many molecular changes that characterise cancer, alterations of intracellular calcium ( $\text{Ca}^{2+}$ ) signalling have been identified as a crucial driver (Colomer and Means, 2007). In particular,  $\text{Ca}^{2+}$  has been reported as a key factor in cellular proliferation (Roderick and Cook, 2008; Shapovalov et al, 2013) and in cellular adhesion (Weinberg, 2013). Here, we formulate and analyse for the first time a model that describes the evolution of a cancer cell density incorporating the effects of  $\text{Ca}^{2+}$  in the adhesion and proliferation processes.

Rising levels of intracellular  $\text{Ca}^{2+}$  have been shown to increase the proliferation of cancer cells in various cancer types such as breast and prostate cancer, melanoma, hepatocellular and non-small-cell lung carcinoma (Prevarskaya et al, 2014, 2018). Experiments (Simpson and Arnold, 1986; Taylor and Simpson, 1992) have shown that increasing extracellular  $\text{Ca}^{2+}$  levels increased intracellular calcium  $\text{Ca}^{2+}$  levels, which increased the cell number and the DNA synthetic ability of cell lines.

Cellular adhesion is mediated through cadherins, which are transmembrane proteins and belong to the class of calcium-dependent cell adhesion molecules (CAMs) (Weinberg, 2013). As an example, consider epithelial cells, which bind to each other by linking the extracellular domains of E-cadherins (Morales et al, 2002). The cytosolic domain of E-cadherin binds to  $\beta$ -catenin, which in turn binds to the cytoskeleton. Changes in the function of  $\beta$ -catenin result in the loss of the ability of E-cadherin to sustain sufficient cell-cell adhesion (Makena and Rao, 2020; Wijnhoven et al, 2000), while alterations in any type of cadherin expression may affect cell adhesion and signal transduction (Cavallaro et al, 2002). Intracellular  $\text{Ca}^{2+}$  directly impacts on the dynamics of both cadherins and catenins (Ko et al, 2001). Moreover, Hills et al (2012) have shown that activation of extracellular  $\text{Ca}^{2+}$ -sensing receptors leads to an increase in E-cadherin expression and an increase in the binding of  $\beta$ -catenin. In cancer, disrupted cell-cell adhesion due to abnormal expression of cadherins and their associated catenins has been linked to metastasis (Morales et al, 2002). For instance, (Byers et al, 1995; Cavallaro and Christofori, 2004) have shown a reduced expression of cadherins in various cancer types, including melanoma, prostate, breast cancer, invasive carcinomas and carcinoma cell lines, and cancers of epithelial origin, when  $\text{Ca}^{2+}$  levels are increased. This results in a reduced force between cells and consequently to cell migration. These results are in line with findings that show that altering CAM function in metastatic cancer cells blocked their ability to invade healthy tissue and move to secondary sites (Kotteas et al, 2014; Naik et al, 2008; Slack-Davis et al, 2009; Zhu et al, 1992). Taken together, the combined changes in cell-cell adhesion and the increase in the proliferation rate and their dependence on  $\text{Ca}^{2+}$  are important mechanisms in cancer and enhance the formation of cancer cell clusters/aggregations that can migrate in a collective manner, a process critical for cancer progression (Friedl et al, 2004; Glinsky et al, 2003; Knútsdóttir et al, 2014).

$\text{Ca}^{2+}$  signalling uses an extensive molecular repertoire of signalling components termed the  $\text{Ca}^{2+}$  signalling "toolkit" (Berridge et al, 2000). A key feature of  $\text{Ca}^{2+}$  signalling is  $\text{Ca}^{2+}$  release from the Endoplasmic Reticulum (ER) to the cytosol through inositol-1,4,5-trisphosphate ( $\text{InsP}_3$ ) receptors ( $\text{InsP}_3\text{Rs}$ ). Together with  $\text{Ca}^{2+}$  resequestration from the cytosol through sarco-endoplasmic  $\text{Ca}^{2+}$  ATPase (SERCA) pumps, a process known as calcium-induced-calcium release can give rise to intracellular  $\text{Ca}^{2+}$  oscillations (Berridge and Galione, 1988; Berridge et al, 2000; Parekh, 2011; Dupont and Combettes, 2016; Thul et al, 2008; Dupont et al, 2011a, 2016a; Schuster et al, 2002; Uhlén and Fritz, 2010; Powell et al, 2020; Sneyd et al, 2017). In addition,  $\text{Ca}^{2+}$  can spread across a population of cells, forming an intercellular  $\text{Ca}^{2+}$  wave (Bereiter-Hahn

(2005); Charles et al (1993, 1991, 1992); Deguchi et al (2000); Narciso et al (2017); Sanderson and Sleight (1981); Yang et al (2009); Young et al (1999)).

Mathematical models of intracellular  $\text{Ca}^{2+}$  oscillations vary substantially in their complexity, ranging from two coupled nonlinear ordinary differential equations (ODEs) to three-dimensional hybrid partial differential equations (PDEs) — see (Dupont et al, 2016a; Falcke et al, 2018) for recent perspectives. In the present study, we employ the model developed in (Atri et al, 1993), which for simplicity we will call the ‘Atri model’. The Atri model is a so-called ‘minimal’ model consisting of only two ODEs that can generate non-linear relaxation oscillations at constant  $\text{InsP}_3$  concentrations (Dupont et al, 2016b; Keener and Sneyd, 2009a,b). Importantly, the Atri model most consistently described hormone-induced  $\text{Ca}^{2+}$  oscillations in HeLa cells (an immortal cell line derived from cervical cancer cells), compared to seven other minimal models for intracellular  $\text{Ca}^{2+}$  oscillations (Estrada et al, 2016). In addition, the mathematical structure of the Atri model allows us to determine analytically the parameter range sustaining calcium oscillations and other bifurcations of the system — see (Atri et al, 1993; Kaouri et al, 2019). Despite its simplicity, the Atri model generates prototypical  $\text{Ca}^{2+}$  signals such as  $\text{Ca}^{2+}$  oscillations and action potentials which correspond to periodic wave trains and solitary pulses, respectively, when  $\text{Ca}^{2+}$  diffusion is taken into account. The Atri model is, hence, sufficient for our modelling framework since our focus is on studying cancer cell movement with  $\text{Ca}^{2+}$  signals as input.

We base our model for the cancer cell density on previously published work (Armstrong et al (2006); Bitsouni et al (2017, 2018); Bitsouni and Eftimie (2018); Chaplain et al (2011); Dyson et al (2016); Domschke et al (2014); Eftimie et al (2017); Gerisch and Chaplain (2008); Gerisch and Painter (2010); Green et al (2010); Hillen and Buttenschön (2019); Painter et al (2015); Shuttleworth and Trucu (2019); Szymańska et al (2009)). These models include nonlinear PDEs with reaction terms for cell growth/proliferation and a non-local advection term, describing cell-cell adhesion. The latter is expressed as an integral term that describes how a cell at position  $\mathbf{x}$  adheres to other cells at position  $\mathbf{x} \pm \mathbf{s}$ , for some  $s > 0$  within the cell’s sensing radius (Armstrong et al, 2006). In the present work, both the rate of cell proliferation and the strength of adhesion are taken to be  $\text{Ca}^{2+}$ -dependent. It is worth noting that additional molecular components and processes could be included. For instance, integrins and TGF- $\beta$  proteins are explicitly represented in (Bitsouni et al, 2018; Engwer et al, 2017) and (Bitsouni et al, 2017; Eftimie et al, 2017), respectively. Moreover, collagen-controlled cell-matrix adhesion, where  $\text{Ca}^{2+}$  is considered as constant, has been developed in (Shuttleworth and Trucu, 2019), while (Ramis-Conde et al, 2008, 2009) studied cadherin-dependent cellular adhesion in an individual-cell-based multiscale model. However, since our study explores the impact of intracellular  $\text{Ca}^{2+}$  on cancer cell movement, we focus on diffusion, cell-cell adhesion and proliferation, the core components of cancer cell behaviour.

The structure of the paper is as follows. In Section 2 we formulate a new model that captures the crucial role of  $\text{Ca}^{2+}$  signalling in cancer by incorporating  $\text{Ca}^{2+}$ -dependent adhesion and proliferation effects. In Section 3 we perform a linear stability analysis and show the ability of the model to generate ADIs and hence cell aggregations. In Section 4 we solve the model numerically. We present various types of aggregation patterns, as well as travelling wave patterns. Taken together, our work provides new insights into the connection between  $\text{Ca}^{2+}$  signalling and cancer cell movement, and suggests a mechanistic approach that can contribute to developing  $\text{Ca}^{2+}$ -transport-targeting tools for cancer diagnosis and treatment (Prevarskaya et al, 2013, 2014).

## 2 A non-local model for calcium signalling in cancer

We denote by  $u(x, t)$  the cancer cell density, by  $c(x, t)$  the cytosolic  $\text{Ca}^{2+}$  concentration and  $h(x, t)$  is the fraction of  $\text{InsP}_3\text{Rs}$  on the ER that have not been inactivated by  $\text{Ca}^{2+}$ . Then the model takes the form

$$\frac{\partial c}{\partial t} = D_c \frac{\partial^2 c}{\partial x^2} + J_{\text{ER}} - J_{\text{pump}}, \quad (2.1a)$$

$$\tau_h \frac{\partial h}{\partial t} = \frac{k_2^2}{k_2^2 + c^2} - h, \quad (2.1b)$$

$$\frac{\partial u}{\partial t} = D_u \frac{\partial^2 u}{\partial x^2} - \frac{\partial}{\partial x} (uF[c, u]) + f(c, u), \quad (2.1c)$$

where

$$J_{\text{ER}} = k_f \mu([\text{InsP}_3]) h \frac{bk_1 + c}{k_1 + c} \quad \text{and} \quad J_{\text{pump}} = \frac{\gamma c}{k_\gamma + c}.$$

Equations (2.1a) and (2.1b) are the spatially extended Atri model for  $\text{Ca}^{2+}$  signalling. In equation (2.1a) the term  $J_{\text{ER}}$  is the flux of  $\text{Ca}^{2+}$  from the ER into the cytosol through  $\text{InsP}_3\text{Rs}$ , where the constant  $k_f$  is the calcium flux when all  $\text{InsP}_3\text{Rs}$  are open and activated,  $b$  is a basal current through the  $\text{InsP}_3\text{Rs}$ , and  $\mu([\text{InsP}_3]) = [\text{InsP}_3]/(k_\mu + [\text{InsP}_3])$  is the fraction of the  $\text{InsP}_3\text{Rs}$  that have  $\text{InsP}_3$  bound and is an increasing function of  $[\text{InsP}_3]$ . In the spatially clamped Atri model relaxation oscillations can be sustained at constant  $[\text{InsP}_3]$ , and  $\mu$  is a bifurcation parameter (see Atri et al (1993); Kaouri et al (2019) for representative bifurcation diagrams).  $J_{\text{pump}}$  is the  $\text{Ca}^{2+}$  flux through the SERCA pumps where  $\gamma$  is the maximal pump rate and  $k_\gamma$  is the  $\text{Ca}^{2+}$  concentration at which the pump rate is at half-maximum. In equation (2.1b) the time constant  $\tau_h > 1\text{s}$  represents the slower time-scale of the inactivation of the  $\text{InsP}_3\text{R}$  by  $\text{Ca}^{2+}$  compared to its activation (Atri et al, 1993; Dupont et al, 2016b). Equation (2.1c) is a non-local, non-linear PDE for the cell density that combines diffusion, cell-cell adhesion (advection) and proliferation (see Domschke et al (2014) and references therein). All parameter values can be found in Tables 1 and 2.

### 2.1 Effect of $\text{Ca}^{2+}$ on cell proliferation

The role of  $\text{Ca}^{2+}$  signals in the proliferation of cancer cells is cancer type specific due to differences in the behaviour of the  $\text{Ca}^{2+}$ -conducting channels and pumps (Monteith et al, 2017). Here, we assume that  $\text{Ca}^{2+}$  enhances the proliferation rate since it has been shown that  $\text{InsP}_3\text{Rs}$  are upregulated in cancer (Monteith et al, 2007, 2017), leading to an enhanced proliferation and survival in all types of cancer (Cárdenas et al, 2016; Prevarskaya et al, 2018; Rezuchova et al, 2019; Tsunoda et al, 2005). Moreover, assuming that cancer cells proliferate in a logistic manner (to describe the observed slow-down in tumour growth following the loss of nutrients (Laird, 1964)), we choose the growth function  $f(c, u)$  as

$$f(c, u) = r_1 \left(1 + g(c)\right) u \left(1 - \frac{u}{k_u}\right), \quad (2.2)$$

where  $r_1$  is the basal growth rate of  $u$  and  $k_u$  is the carrying capacity. The  $\text{Ca}^{2+}$ -dependent function  $g(c)$  describes the enhanced proliferation of cancer cells that is associated with a major re-arrangement of  $\text{Ca}^{2+}$  pumps,  $\text{Na}^+/\text{Ca}^{2+}$  exchangers and  $\text{Ca}^{2+}$  channels (Capiod et al, 2007; Simpson and Arnold, 1986; Taylor and Simpson, 1992); we assume that it is given by

$$g(c) = \frac{r_2 c^2}{r_3 + c^2}, \quad (2.3)$$

i.e. it saturates as  $c$  increases and vanishes at  $c = 0$ . We choose  $r_1$ ,  $r_2$  and  $r_3$  based on experimental evidence, as follows. For  $r_1$  it was shown that doubling times for cancer cells range from 1 – 10 days (Cunningham

and You, 2015; Morani et al, 2014). In Panetta et al (2000) the doubling time for breast and ovarian cancer ranges between 0.25 – 7 days. Here we choose as doubling time 7 days.  $r_2$ , the highest reaction rate that can be achieved at saturating  $\text{Ca}^{2+}$  concentrations, and the half-maximal  $\text{Ca}^{2+}$  concentration constant,  $r_3$ , are based on experimental evidence in (Simpson and Arnold, 1986; Taylor and Simpson, 1992). All parameter values can be found in Tables 1 and 2.

## 2.2 Effect of $\text{Ca}^{2+}$ on cell-cell adhesion

Cancer cells often show a decrease in cell-cell adhesion compared to healthy cells, which correlates with tumour invasion and metastasis (Cavallaro and Christofori, 2001; Makena and Rao, 2020). When adhesive bonds are formed and broken a cell-cell adhesion-mediated directed cancer cell migration occurs as a result of cellular attraction and repulsion. The cell-cell adhesion forces are created through the binding of adhesive molecules such as cadherins (Byers et al, 1995; Kim et al, 2011; Panorchan et al, 2006), see Section 1. Thus, we consider a calcium-dependent adhesion term in a bounded domain  $\Omega = [0, R_s]$  in the cell density equation (2.1c) where the non-local cell-cell interactions are described by a function that depends on cell density and  $\text{Ca}^{2+}$ ,

$$F[c, u] = \frac{S(c(x, t))}{R_s} \int_0^{R_s} K_{\text{int}}(r) \left( u(x+r, t) - u(x-r, t) \right) dr,$$

where  $K_{\text{int}} \in L^\infty(\Omega)$  is the interaction kernel between cancer cells, with  $\partial_x K_{\text{int}} \in L^\infty(\Omega)$ , and  $S(c)$  the adhesion strength function, which depends on  $\text{Ca}^{2+}$ .  $R_s > 0$  is the cell sensing ‘radius’, i.e. the maximum range over which a cell can detect surrounding cells (Armstrong et al, 2006). Here, we assume that  $R_s$  equals five times the length of an average cell (Armstrong et al, 2006; Gerisch and Chaplain, 2008). Biologically this represents the extent of the cell’s protrusions, e.g. filopodia. We define an attraction-repulsion kernel (see (Eftimie et al, 2007, 2017)) as

$$K_{\text{int}}(x) = q_a K_a(x) - q_r K_r(x),$$

with  $q_a$  and  $q_r$  describing the magnitude of attractive and repulsive interactions, respectively, and  $K_a(x)$  and  $K_r(x)$  denoting the spatial range over which these interactions take place. We will take the kernel to be attractive at medium/long ranges (i.e. at the edges of the cell) ensuring cell cohesion, and repulsive at very short ranges (i.e. over the cell surface) to represent cell volume-exclusion effects and thus prevent unrealistically high cell densities (Palachanis et al, 2015). Throughout the rest of this study, we consider Gaussian attraction and repulsion kernelw (Eftimie et al, 2007) so that

$$K_{\text{int}}(x) = \frac{q_a}{\sqrt{2\pi m_a^2}} e^{-\frac{(x-s_a)^2}{2m_a^2}} - \frac{q_r}{\sqrt{2\pi m_r^2}} e^{-\frac{(x-s_r)^2}{2m_r^2}}, \quad (2.4)$$

where  $s_a$  and  $s_r$  represent the location of maximal attraction and repulsion, respectively, with  $s_r < s_a < R_s$ . The constants  $m_j = s_j/8$ ,  $j = a, r$ , represent the widths of the interaction kernels, respectively. They are chosen such that the support of more than 98% of the mass of the kernels is inside the interval  $[0, \infty)$

As discussed in Section 1, expression of  $\text{Ca}^{2+}$ -dependent cell-cell adhesion molecules is reduced in several human cancer types when  $\text{Ca}^{2+}$  levels are increased (Byers et al, 1995; Cavallaro and Christofori, 2004), which leads to a decreased adhesive force between the cells. A biologically realistic choice for the adhesion strength function is thus

$$S(c) = s^* \left( 1 - \frac{a_1 c}{a_2 + c} \right) \quad (2.5)$$

an inverse Hill function for  $c$  that tends to zero for large  $c$  values. We estimated the parameters  $a_1, a_2$  and  $s^*$  so that the adhesive force exhibits a biologically sensible response to  $\text{Ca}^{2+}$  variations (for parameter values see Table 2).

### 2.3 Non-dimensionalized model

To non-dimensionalize the model (2.1), we define the following quantities:

$$\begin{aligned} \tilde{t} &= \frac{t}{\tau_h}, & \tilde{x} &= \frac{x}{L_0}, & \tilde{c} &= \frac{c}{k_1}, & \tilde{u} &= \frac{u}{k_u}, & \tilde{R}_s &= \frac{R_s}{L_0}, & \tilde{q}_a &= k_u q_a, & \tilde{q}_r &= k_u q_r, \\ & & & & \tilde{S}(\tilde{c}) &= \frac{\tau_h}{L_0^2} S(k_1 \tilde{c}). \end{aligned}$$

The length scale,  $L_0$ , is defined as the typical cell size/diameter of an average cancer cell. Cancer cells can be smaller or bigger than healthy cells depending on several factor including the cancer type. HeLa cells, for example, are around  $40\mu\text{m}$  in diameter, while they measure  $20\mu\text{m}$  in their naturally compressed state (Boulter et al, 2006; Puck et al, 1956). Generally, the average cancer cell diameter is between  $20 - 30\mu\text{m}$  (Ha and Bhagavan, 2011). Here, we choose  $L_0 = 20\mu\text{m}$ , while we set the time scale as  $\tau_h = 2\text{s}$  (Kaouri et al, 2019). In addition, we rescale the cell density with the cell carrying capacity,  $k_u$ , taken to be  $\sim 6.7 \cdot 10^7 \text{cell/volume}$  (Gerisch and Chaplain, 2008). We obtain the dimensionless parameters:

$$\begin{aligned} \tilde{D}_c &= \frac{D_c \tau_h}{L_0^2}, & K_1 &= \frac{k_f \tau_h}{k_1}, & \Gamma &= \frac{\gamma \tau_h}{k_1}, & K &= \frac{k_\gamma}{k_1}, & K_2 &= \frac{k_2}{k_1}, \\ \tilde{D}_u &= \frac{D_u \tau_h}{L_0^2}, & \tilde{r}_1 &= r_1 \tau_h, & \tilde{r}_3 &= \frac{r_3}{k_1^2}. \end{aligned}$$

We also briefly discuss the choice of the diffusion coefficients. It has been shown in (Allbritton et al, 1992) that the diffusion coefficient of free cytosolic  $\text{Ca}^{2+}$  is  $2.23 \cdot 10^{-6} \text{cm}^2 \text{s}^{-1}$ . The action of omnipresent  $\text{Ca}^{2+}$  buffers can be subsumed into an effective  $\text{Ca}^{2+}$  diffusion coefficient, which we here set to  $D_c = 0.2 \cdot 10^{-6} \text{cm}^2 \text{s}^{-1}$ . Assuming that the delay of  $\text{Ca}^{2+}$  propagation through gap junctions joining cells is negligible, we arrive at  $\tilde{D}_c = 0.1$ . The diffusion coefficient of cancer cells is in the range of  $10^{-11} - 10^{-9} \text{cm}^2 \text{s}^{-1}$  (Bray, 1992; Chaplain and Lolas, 2006; Franssen et al, 2019). This corresponds to dimensionless values of  $\tilde{D}_u$  between  $5 \cdot 10^{-6} - 5 \cdot 10^{-3}$ . We choose  $\tilde{D}_u = 0.0025$ . All other model parameters are given in Tables 1 and 2.

As in (Domschke et al, 2014), we introduce the dimensionless functions  $\tilde{K}_{a,r}(\tilde{r}) = L_0 K_{a,r}(L_0 \tilde{r}) = L_0 K_{a,r}(r)$  so that

$$\tilde{K}_{\text{int}}(\tilde{r}) = L_0 k_u (q_a K_a(r) - q_r K_r(r)).$$

Therefore, we have for the non-local term

$$\begin{aligned} F[c, u](x, t) &= \\ &= \frac{L_0}{\tau_h \tilde{R}_s} \tilde{S}(\tilde{c}) \tilde{q}_a \int_0^{\tilde{R}_s} \left( \tilde{K}_a(\tilde{r}) - \frac{\tilde{q}_r}{\tilde{q}_a} \tilde{K}_r(\tilde{r}) \right) (\tilde{u}(\tilde{x} + \tilde{r}, \tilde{t}) - \tilde{u}(\tilde{x} - \tilde{r}, \tilde{t})) d\tilde{r} \\ &= \frac{L_0}{\tau_h \tilde{R}_s} \tilde{s}^* \tilde{q}_a \tilde{F}[\tilde{c}, \tilde{u}](\tilde{x}, \tilde{t}) = F_0 \tilde{F}[\tilde{c}, \tilde{u}], \end{aligned}$$

where  $F_0 = L_0 \tilde{s}^* \tilde{q}_a / (\tau_h \tilde{R}_s)$  is the typical cancer cell speed.

Clark and Vignjevic (2015) showed that cancer cell speeds cannot exceed  $10\mu\text{m}/\text{min}$ . We Consider the typical cancer cell speed,  $F_0$ , to vary between  $1\mu\text{m}/\text{min}$  and  $10\mu\text{m}/\text{min}$  to account for various cancer types which are characterised by slower or faster cells (e.g. for A375M2 human melanoma the speed ranges between  $0.5 - 10\mu\text{m}/\text{min}$ , and for MDA-MB-231 breast cancer it ranges between  $0.4 - 4.2\mu\text{m}/\text{min}$ ). We find that the ratio  $\tau_h F_0 / L_0$  is in the range

$$0.0017 \leq \frac{\tau_h}{L_0} F_0 \leq 0.017,$$

leading to

$$0.008 \leq \tilde{s}^* \tilde{q}_a \leq 0.08. \quad (2.6)$$

This provides bounds for the value of  $\tilde{s}^* \tilde{q}_a$  we are going to choose in Sections 3 and 4.

After dropping the tildes for notational convenience, we obtain the following non-dimensional system:

$$\frac{\partial c}{\partial t} = D_c \frac{\partial^2 c}{\partial x^2} + \mu K_1 h \frac{b+c}{1+c} - \frac{\Gamma c}{K+c}, \quad (2.7a)$$

$$\frac{\partial h}{\partial t} = \frac{1}{1+c^2} - h, \quad (2.7b)$$

$$\frac{\partial u}{\partial t} = D_u \frac{\partial^2 u}{\partial x^2} - \frac{\tau_h}{L_0} F_0 \frac{\partial}{\partial x} (u(F[c, u])) + r_1 \left( 1 + \frac{r_2 c^2}{r_3 + c^2} \right) u(1-u). \quad (2.7c)$$

Although  $D_u = 0.0025$ , which corresponds to a large diffusion value, the behaviour of cancer cells is still advection-dominated. This directed, advective movement of cancer cells results from the aforementioned cell-cell adhesion forces and from an elevated macrophage density near highly mutated cancer cells (Lin et al, 2006), which decreases the random movement of the cancer cells (Goswami et al, 2005; Hagemann et al, 2005).

Table 1: Model parameters, dimensional values, non-dimensional values and relevant references.

Param.	Description	Dim. value	Non-dim. value	Reference
$D_c$	Diffusion coefficient of $\text{Ca}^{2+}$	$20\mu\text{m}^2\text{s}^{-1}$	0.1	Atri et al (1993); Höfer et al (2001); Wilkins and Sneyd (1998)
$b$	Fraction of activated $\text{InsP}_3\text{Rs}$ receptors when $[\text{Ca}^{2+}] = 0$	-	0.111	Atri et al (1993)
$k_1$	$K_m$ (Michaelis constant) for activation of $\text{InsP}_3\text{Rs}$ receptors by $\text{Ca}^{2+}$	$0.7\mu\text{M}$	1	Atri et al (1993); Kaouri et al (2019)
$k_f$	$\text{Ca}^{2+}$ flux when all $\text{InsP}_3\text{Rs}$ receptors are open and activated	$16.2\mu\text{Ms}^{-1}$	$K_1 = 324/7$	Atri et al (1993); Kaouri et al (2019)
$k_\mu$	$K_m$ (Michaelis constant) for binding of $\text{InsP}_3$ to its receptor	$0.7\mu\text{M}$	1	Atri et al (1993); Kaouri et al (2019)
$\gamma$	Maximum rate of pumping of ER $\text{Ca}^{2+}$	$2\mu\text{Ms}^{-1}$	$\Gamma = 40/7$	Atri et al (1993)
$k_\gamma$	$[\text{Ca}^{2+}]_c$ at which the rate of $\text{Ca}^{2+}$ pumping from the cytosol is at half-maximum	$0.1\mu\text{M}$	$K = 1/7$	Atri et al (1993); Kaouri et al (2019)
$k_2$	$K_m$ (Michaelis constant) for inactivation of $\text{InsP}_3$ receptors by $\text{Ca}^{2+}$	$0.7\mu\text{M}$	$K_2 = 1$	Atri et al (1993); Kaouri et al (2019)
$D_u$	Diffusion coefficient of cancer cells	$0.5\mu\text{m}^2\text{s}^{-1}$	0.0025	Bray (1992); Chaplain and Lolas (2006); Enderling et al (2006); Franssen et al (2019)
$R_s$	Sensing radius	$100\mu\text{m}$	5	Armstrong et al (2006); Gerisch and Chaplain (2008)

*Continued on next page*

Table 1 – *Continued from previous page*

Param.	Description	Dim. value	Non-dim. value	Reference
$k_u$	Carrying capacity of the cancer cell population	$6.7 \cdot 10^7$ cells/cm <sup>3</sup>	1	Gerisch and Chaplain (2008)
$r_1$	Growth rate of the cancer cell population	7 days (doubling time)	0.1	Cunningham and You (2015); Morani et al (2014); Panetta et al (2000)

Table 2: Estimated model parameters, non-dimensional values and relevant references.

Param.	Description	Non-dim. value	Reference
$q_a$	Magnitude of attraction	0 – 0.44	Guided by linear stability analysis (Section 3.2) and the range (2.6), based on Clark and Vignjevic (2015)
$q_r$	Magnitude of repulsion	0 – 0.44	Guided by linear stability analysis (Section 3.2)
$s_a$	Attraction range	1	Bitsouni and Eftimie (2018)
$s_r$	Repulsion range	0.25	Bitsouni et al (2017, 2018); Bitsouni and Eftimie (2018)
$m_a$	Width of attraction kernel	1/8	Bitsouni and Eftimie (2018)
$m_r$	Width of repulsion kernel	1/32	Bitsouni et al (2017, 2018); Bitsouni and Eftimie (2018)
$s^*$	Magnitude of cell-cell adhesion forces of the cancer cell population	1	Armstrong et al (2006); Bitsouni et al (2017, 2018); Gerisch and Chaplain (2008)
$a_1$	Lowest value of cell-cell strength due to increase in $[\text{Ca}^{2+}]$	0.5	Estimated
$a_2$	Half-minimum ( $K_m$ ) $[\text{Ca}^{2+}]$	0.5	Estimated
$r_2$	Largest reaction value at saturating $[\text{Ca}^{2+}]$	1.6	Simpson and Arnold (1986); Taylor and Simpson (1992)
$r_3$	Half-maximal $[\text{Ca}^{2+}]$	4	Simpson and Arnold (1986); Taylor and Simpson (1992)



### 3 Analytical results

#### 3.1 Existence of solution

The existence of a unique global-in-time classical solution of the model (2.1) can be proven using the theory of semigroups (Henry, 1981), within the framework of ODEs. The proof of the theorem follows the same steps as (Bitsouni et al, 2017; Chaplain et al, 2011).

#### 3.2 Linear stability analysis

In our model an instability of a spatially homogeneous state can arise when advection effects increase; we will call this an advection-driven instability (ADI). The loss of stability leads to spatial patterns, which biologically correspond to cell aggregations (Keller and Segel, 1970).

In this section, we linearise the model (2.7) and investigate the conditions for ADIs. The spatially homogeneous steady states  $(c^*, h^*, u^*)$  of the system (2.7) are given by

$$\left(c^*, \frac{1}{1+c^{*2}}, 0\right) \quad \text{and} \quad \left(c^*, \frac{1}{1+c^{*2}}, 1\right), \quad (3.1)$$

with  $c^* \geq 0$  determined by the solution of the quartic equation

$$c^{*4} + c^{*3} + \left(1 - \mu \frac{K_1}{\Gamma}\right) c^{*2} + \left(1 - \mu \frac{K_1}{\Gamma} (K + b)\right) c^* - \mu \frac{K_1}{\Gamma} K b = 0.$$

We seek conditions for a steady state  $(c^*, h^*, u^*)$  to become unstable due to ADI. We thus consider small perturbations to the steady state,  $(\bar{c}, \bar{h}, \bar{u})$ , such that  $c(x, t) = c^* + \bar{c}(x, t)$ ,  $h(x, t) = h^* + \bar{h}(x, t)$ ,  $u(x, t) = u^* + \bar{u}(x, t)$ . Substituting these into (2.7), linearising around the spatially uniform steady state, and using the notation  $\bar{y} = (\bar{c}, \bar{h}, \bar{u})$ , we obtain

$$\frac{\partial \bar{y}}{\partial t} = D \frac{\partial^2 \bar{y}}{\partial x^2} - \frac{\partial J_a}{\partial x} + J_r \bar{y},$$

where  $D$  is a diagonal matrix with entries  $(D_c, 0, D_u)$  and  $J_a = (0, 0, \alpha)$ , with

$$\alpha = \frac{u^*}{R_s} S(c^*) \int_0^{R_s} K_{\text{int}}(r) (\bar{u}(x+r, t) - \bar{u}(x-r, t)) dr,$$

and

$$J_r = \begin{bmatrix} J_2(c^*, h^*) & 0 \\ r_1 u^* (1 - u^*) \frac{2r_2 r_3 c^*}{r_3 + c^{*2}} & 0 \\ 0 & r_1 (1 - 2u^*) \left(1 + \frac{r_2 c^{*2}}{r_3 + c^{*2}}\right) \end{bmatrix},$$

where

$$J_2 = \begin{bmatrix} \mu K_1 h \frac{1-b}{(1+c^*)^2} - \frac{\Gamma K}{(K+c^*)^2} & \mu K_1 \frac{b+c^*}{1+c^*} \\ -\frac{2c^*}{(1+c^{*2})^2} & -1 \end{bmatrix},$$

is the Jacobian of the linearised Atri model. We seek solutions of the form  $\bar{y} = w e^{i\xi x + \lambda t}$ , where  $w = (A_c, A_h, A_u)$  with  $|A_c|, |A_h|, |A_u| \ll 1$ . The wave number and frequency of the perturbations are denoted by  $\xi$  and  $\lambda$ , respectively. We then find

$$\lambda w = (J_d + J_r) w,$$

with

$$J_d = \begin{bmatrix} -D_c \xi^2 & 0 & 0 \\ 0 & 0 & 0 \\ 0 & 0 & -D_u \xi^2 + 2\xi u^* \widehat{K}_{\text{int}}^s(\xi) S(c^*) / R_s, \end{bmatrix}$$

where  $\widehat{K}_{\text{int}}^s(\xi) = \int_0^{R_s} K_{\text{int}}(r) \sin(\xi r) dr$  is the Fourier sine transform of  $K_{\text{int}}(r)$ .

Since the cell density equation (2.7c) is not coupled to the Atri equations (2.7a) and (2.7b), the matrix  $M = J_d + J_r$  has a block structure and the eigenvalues of  $M$  are split into those of the (linearised) Atri model and that of the (linearised) cancer cell density equation. Hence, to identify ADIs we only need to study the linear stability of the cell density equation, i.e. the eigenvalue (dispersion relation)

$$\lambda_u(\xi, c^*) = -D_u \xi^2 + \frac{2\xi u^*}{R} S(c^*) \widehat{K}_{\text{int}}^s(\xi) + r_1 (1 - 2u^*) \left( 1 + \frac{r_2 c^{*2}}{r_3 + c^{*2}} \right),$$

which for the Gaussian attraction and repulsion kernels given in (2.4) becomes

$$\begin{aligned} \lambda_u(\xi, c^*) = & -D_u \xi^2 + \frac{2\xi u^*}{R} S(c^*) \left( e^{-\frac{(\xi m_a)^2}{2}} \sin(\xi s_a) - \frac{q_r}{q_a} e^{-\frac{(\xi m_r)^2}{2}} \sin(\xi s_r) \right) \\ & + r_1 (1 - 2u^*) \left( 1 + \frac{r_2 c^{*2}}{r_3 + c^{*2}} \right). \end{aligned} \quad (3.2)$$

Solutions with  $\lambda_u > 0$  are unstable and grow exponentially in time, corresponding to pattern formation and cell aggregation in the non-linear system (Murray, 2003; Painter et al, 2015). For  $u^* = 0$  and  $\xi = 0$ , we obtain

$$\lambda_u^0(0, c^*) = r_1 \left( 1 + \frac{r_2 c^{*2}}{r_3 + c^{*2}} \right) > 0,$$

In contrast, for  $u^* = 1$  and  $\xi = 0$ , we find

$$\lambda_u^1(0, c^*) = -r_1 \left( 1 + \frac{r_2 c^{*2}}{r_3 + c^{*2}} \right) < 0.$$

Here, we use the superscript to indicate the value of  $u^*$ . Note that  $\lambda_u^0(\xi, 0)$  and  $\lambda_u^1(\xi, 0)$  are the eigenvalues of the linearised Fisher's equation when  $q_a = q_r = 0$ . For positive  $q_a$  and  $q_r$  and no calcium,  $\lambda_u^1(\xi, 0)$  becomes positive for some  $\xi > 0$  when the advection strength increases sufficiently. To identify the threshold values of  $q_a$  and  $q_r$ , we present the non-negative contour plots of  $\lambda_u^1(\xi, 0)$  in Fig. 1, where negative values are mapped to zero for better visualisation. In Figs. 1(a)–1(d) we set  $q_a = 0.14$ ,  $q_a = 0.22$ ,  $q_a = 0.33$  and  $q_a = 0.44$ , respectively, while  $q_r$  varies from 0 to 0.44. We observe extended regions with  $\lambda_u^1 > 0$ , which indicate pattern formation in the nonlinear system via ADI. In Figs. 1(b)–1(d) we observe disjoint parameter regions, which grow larger as  $q_a$  increases. Note that we do not need to plot for larger values of  $\xi$  since  $\lambda_u^1(\xi, 0)$  tends to  $-\infty$  as  $\xi$  tends to  $\infty$ .

We next establish the effect of  $\text{Ca}^{2+}$  on ADI. In Fig. 2 we display contour plots corresponding to non-negative values of  $\lambda_u^1(\xi, c^*)$ , for nine different combinations of  $q_a$  and  $q_r$ : (0.14, 0.01), (0.16, 0.01), (0.22, 0.01), (0.33, 0.01), (0.01, 0.22), (0.14, 0.22), (0.22, 0.22), (0.33, 0.33) and (0.44, 0.44). We observe that the ADI regions vanish at sufficiently large values of  $c^*$  for all figures except Figs. 2(d), 2(h) and 2(i). Note that we choose  $0 \leq c^* \leq 2.3$  since 2.3 is the maximum value of the steady state of the Atri model; other  $\text{Ca}^{2+}$  models may achieve higher  $c^*$  levels but we expect a qualitatively similar behaviour. Also, as  $c^*$  increases the range of  $\xi$  in the ADI regions decreases. In Figs. 2(c), 2(d), 2(h) and 2(i) we observe disjoint parameter regions for positive  $\lambda_u^1(\xi, c^*)$ .

The stability of the spatially homogeneous Atri model (determined by the matrix  $J_2$ ) has been covered in detail in (Atri et al, 1993; Kaouri et al, 2019). Hopf bifurcations occur at  $\mu = 0.289$  and  $\mu = 0.495$ , between which stable relaxation oscillations (limit cycles) exist. Action potentials also appear for a very small range of  $\mu$ . Including diffusion leads to the emergence of periodic wave trains and solitary pulses when the Atri model exhibits limit cycles and action potentials, respectively (see Fig. 4).

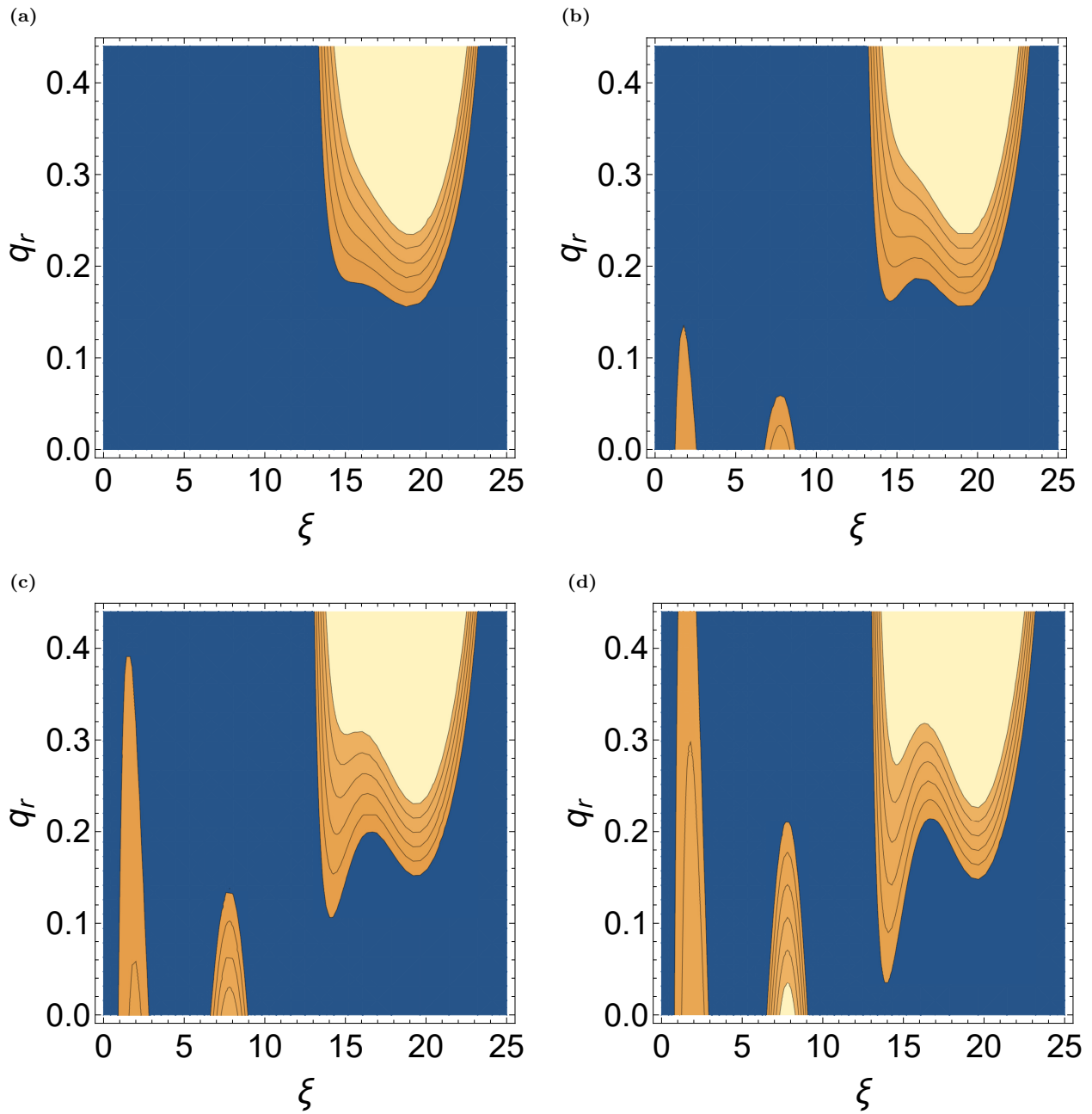


Fig. 1: The contours of non-negative  $\lambda_u^1(\xi, 0)$ , dispersion relation of the linearised cell density equation, for  $c^* = 0$ ,  $u^* = 1$ , which enclose parameter regions corresponding to adhesion-driven instabilities, for: (a)  $q_a = 0.14$  (b)  $q_a = 0.22$  (c)  $q_a = 0.33$  (d)  $q_a = 0.44$ . In (a)–(d)  $q_r$  varies from 0 to 0.44, respectively. The remaining parameter values are given in Tables 1 and 2. Negative values of  $\lambda_u^1(\xi, 0)$  have been set to zero for better visualisation.

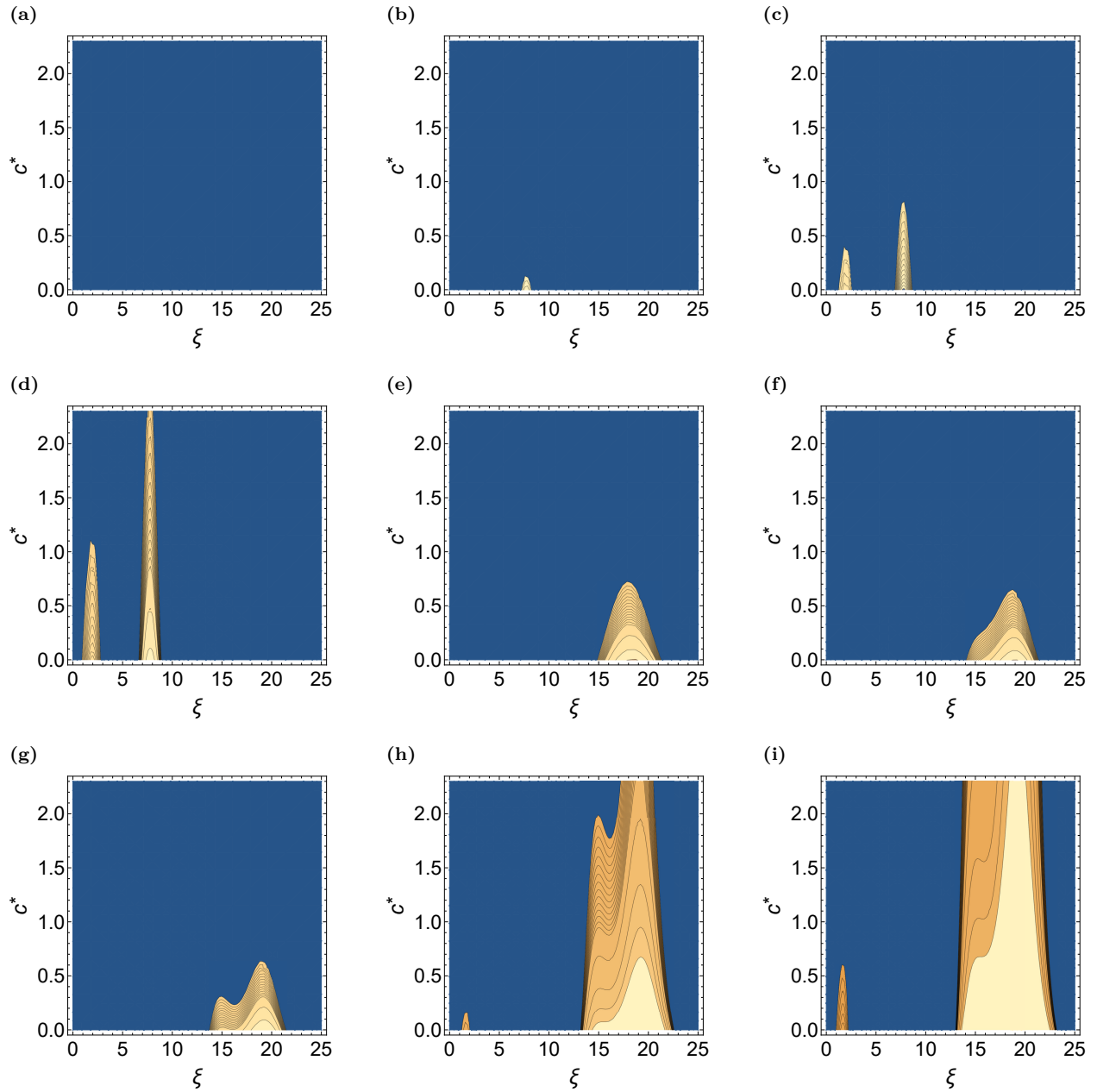


Fig. 2: Contour plots of the dispersion relation  $\lambda_u^1(\xi, c^*)$  as  $c^*$  varies for: (a)  $q_a = 0.14$ ,  $q_r = 0.01$ ; (b)  $q_a = 0.16$ ,  $q_r = 0.01$ ; (c)  $q_a = 0.22$ ,  $q_r = 0.01$ ; (d)  $q_a = 0.33$ ,  $q_r = 0.01$ ; (e)  $q_a = 0.01$ ,  $q_r = 0.22$ ; (f)  $q_a = 0.14$ ,  $q_r = 0.22$ ; (g)  $q_a = 0.22$ ,  $q_r = 0.22$ ; (h)  $q_a = 0.33$ ,  $q_r = 0.33$ ; (i)  $q_a = 0.44$ ,  $q_r = 0.44$ . All other parameter values are given in Tables 1 and 2. Negative values of  $\lambda_u^1(\xi, 0)$  have been set to zero for better visualisation.

## 4 Numerical simulations

In this section we numerically solve model (2.7) using a method-of-lines approach. The domain  $[0, L]$  is discretized into a cell-centered grid with uniform length  $h = 1/N$ , where  $N = 100$  is the number of grid cells per unit length. All simulations are performed with  $L = 120$  and with periodic boundary conditions. The diffusion terms are discretized using a second order centered difference scheme. The advection term is discretized using a third order upwind scheme, augmented with a flux-limiting scheme to ensure the solution's positivity. The non-local term in equation (2.7c) presents challenges regarding its efficient and accurate evaluation. Here we employ the scheme based on the Fast Fourier Transform introduced in (Gerisch, 2010), using the trapezoidal rule to pre-compute the integration weights. The resulting system of ODEs is integrated using the ROWMAP integrator introduced in Weiner et al (1996). We use the implementation<sup>1</sup> provided in (Weiner et al, 1996). The integrator (written in Fortran) was wrapped using f2py into a scipy integrate class (Virtanen et al, 2019). The spatial discretisation (right hand side of ODE) is implemented using NumPy. The integrator's error tolerance is set to  $v_{\text{tol}} = 10^{-7}$ . For the full details of the numerical methods we refer to (Gerisch, 2001; Hundsdorfer and Verwer, 2003).

The initial conditions of the system are taken to be narrow Gaussian functions as follows:

$$c(x, 0) = c^* + 1.42857e^{-0.25(x-\frac{L}{2})^2}, \quad (4.1a)$$

$$h(x, 0) = \frac{1}{1 + c^{*2}}, \quad (4.1b)$$

$$u(x, 0) = e^{-0.25(x-\frac{L}{2})^2}. \quad (4.1c)$$

### 4.1 Adhesion-driven instability, pattern formation and cell aggregations

Each term in the cancer cell density equation (2.7c) critically affects the behaviour of cancer cells. Thus, below we examine the effect of each term in turn and compare the results with those of the linear stability analysis in the absence of  $\text{Ca}^{2+}$ , in Section 3.2. We explore a wide range of values for  $q_a$  (magnitude of attraction) and  $q_r$  (magnitude of repulsion), guided by Fig. 1. For  $q_a$  we also take into account the range of  $q_a$  reported in (2.6)), based on measurements of the speed of cancer cell movement. No experimental evidence was found for  $q_r$  and we consider the same range as for  $q_a$ . We thus examine several possible scenarios and identify various types of patterns and aggregations.

In Fig. 3(a) we plot the cell density for non-zero diffusion and advection but zero proliferation; this represents cells with very slow doubling time. We take  $q_a = 0.22$ ,  $q_r = 0.01$ , i.e. attraction much larger than repulsion. We see that the cancer cells form a single stationary pulse. In Fig. 3(b), we add proliferation, but take zero adhesion (Fisher's equation). The cancer cells exhibit a travelling front that propagates in opposite directions at a constant speed, as expected (Murray, 2003). In Fig. 3(c) we include diffusion, advection and proliferation, with  $q_a = 0.14$  and  $q_r = 0.01$ . We still see a Fisher-like travelling front, consistently with Fig. 1(a) which predicts no ADI for these choices of  $q_a$  and  $q_r$ .

In Fig. 3(d), we further increase the strength of attraction to  $q_a = 0.22$  while keeping  $q_r = 0.01$ , and a pattern emerges behind the travelling front due to ADI, as predicted by Fig. 1(b). It is a "mixed" pattern, featuring merging and emerging peaks; some cancer cells form stationary pulses, while others organise into travelling pulses. This behaviour can be explained by the strong attractive forces that make cells form large aggregations. This type of pattern has been identified in previous work (see Andasari et al (2011); Bitsouni et al (2017); Hillen and Painter (2009); Loy and Preziosi (2019); Eftimie et al (2017); Wang and Hillen (2007)),

In Fig. 3(e), we lower attraction to  $q_a = 0.14$  and increase the magnitude of repulsion to  $q_r = 0.22$ ; the Fisher-like front persists and the pattern behind it now exhibits thin spikes. This can be explained by

<sup>1</sup> [http://www.mathematik.uni-halle.de/wissenschaftliches\\_rechnen/forschung/software/](http://www.mathematik.uni-halle.de/wissenschaftliches_rechnen/forschung/software/)

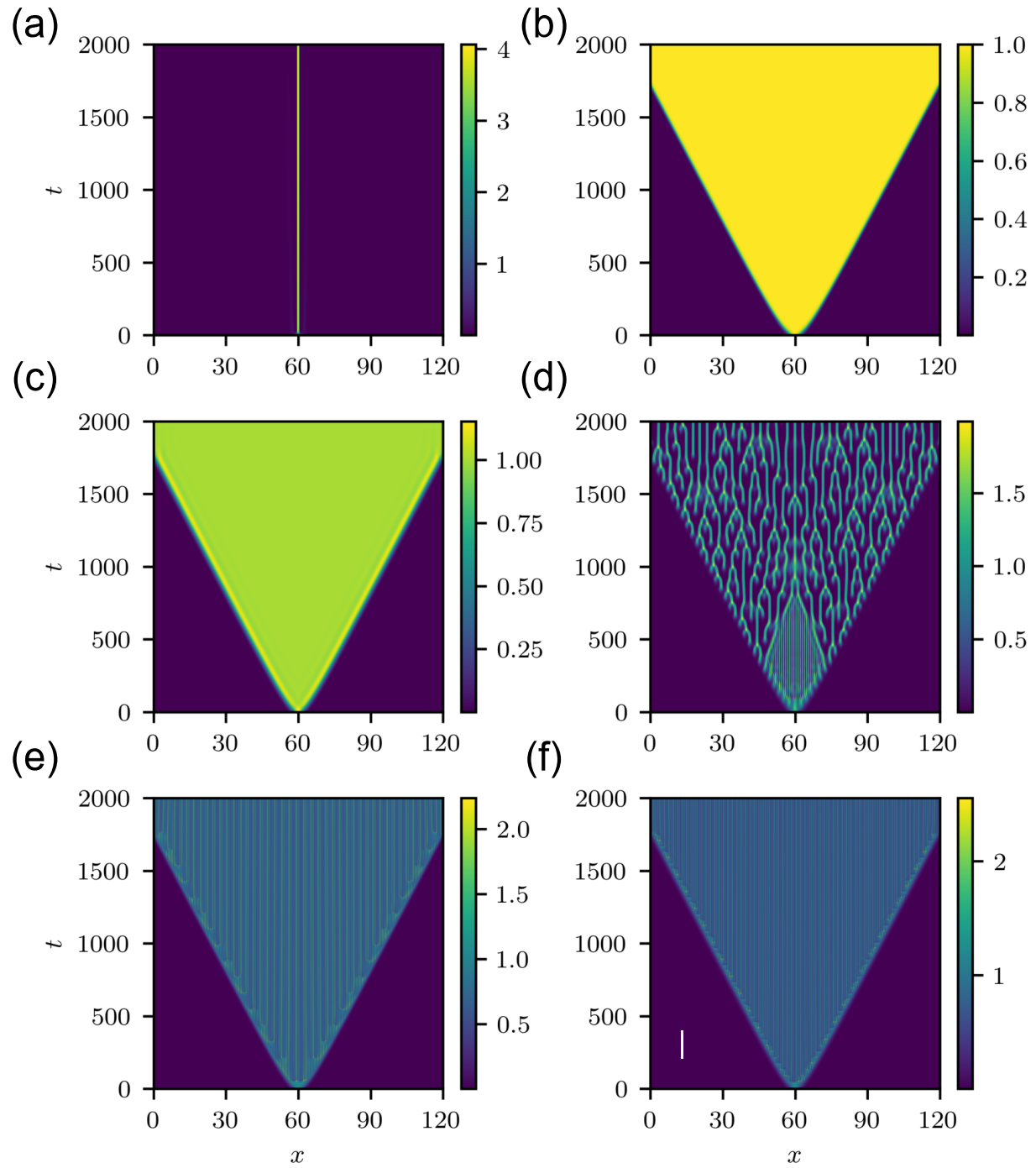


Fig. 3: Cancer cell density,  $u(x, t)$ , for no  $\text{Ca}^{2+}$  effect ( $a_1 = a_2 = r_2 = r_3 = 0$ ), governed by equation (2.7c). The initial conditions are given in (4.1c). (a)  $q_a = 0.22, q_r = 0.01$ , no proliferation; (b)  $q_a = 0, q_r = 0$ ; (c)  $q_a = 0.14, q_r = 0.01$ ; (d)  $q_a = 0.22, q_r = 0.01$ ; (e)  $q_a = 0.14, q_r = 0.22$ ; (f)  $q_a = 0.22, q_r = 0.22$ . All other parameter values as in Tables 1 and 2.

the strong repulsive forces leading to a larger number of smaller aggregations than those in the case where attraction is larger than repulsion, as in Fig. 3(d). This behaviour again agrees with the linear stability analysis (see Fig. 1(b)). Finally, in Fig. 3(f) we take equal attraction and repulsion,  $q_r = q_a = 0.22$ . The pattern is similar to that in Fig. 3(e). Note: in order to see the more detailed features of the Figures the reader is encouraged to follow the electronic version of the paper.

## 4.2 Calcium signals

Here, we investigate the behaviour of the spatially extended Atri model (2.7a) and (2.7b). The four panels in Fig. 4 display the behaviour of the  $\text{Ca}^{2+}$  concentration as we increase  $\mu$ , which is equivalent to increasing the  $\text{InsP}_3$  concentration. For  $\mu = 0.1$ , for which the spatially clamped Atri model possesses a linearly stable fixed point (Atri et al, 1993; Kaouri et al, 2019), Fig. 4(a) illustrates that the initial Gaussian condition decays to this fixed point. Setting  $\mu = 0.288$  leads to a solitary travelling pulse (Fig. 4(b)), while a value of  $\mu$  between the two Hopf bifurcations results in a periodic wave train (Keener and Sneyd, 2009a,b); in Fig. 4(c) we take, as an example,  $\mu = 0.3$ . Finally, for larger values of  $\mu$  the Atri model is linearly stable again and we find a similar pattern to Fig. 4(a), in that the initial condition decays to the steady state, but in a periodic manner. In Fig. 4(d) we take  $\mu = 0.6$  as an example of the latter case. These four types of  $\text{Ca}^{2+}$  signals emerge in almost all  $\text{Ca}^{2+}$  models. Here, we use them as input to the cancer cell density equation (2.7c).

## 4.3 The effect of $\text{Ca}^{2+}$ on the cell density

We now examine the effect of the  $\text{Ca}^{2+}$  signals on the cancer cell density. We fix the attraction and repulsion magnitudes,  $q_a$  and  $q_r$ , and vary  $\mu$ . Fig. 5 (top panel) ( $q_a = 0.14$ ,  $q_r = 0.01$ ) shows a Fisher-like travelling front in all Figs. (a)–(d), irrespective of the  $\text{InsP}_3$  and  $\text{Ca}^{2+}$  levels; this is consistent with the linear stability analysis that predicts no ADI. These results are in line with Fig. 2(a). In contrast, when we increase  $q_a$  to 0.22 in Fig. 5 (bottom panel) small  $\text{InsP}_3$  concentrations ( $\mu = 0.1$  and  $\mu = 0.3$ , respectively) induce a pattern, due to ADI. As we increase the  $\text{InsP}_3$  concentration, the pattern vanishes, as illustrated in Figs. 5(c') and 5(d') which are for  $\mu = 0.45$  and  $\mu = 0.6$ , respectively. These results are in line with Fig. 2(c).

In Figs. 6 we see that for larger values of  $q_a$  ( $q_a = 0.33$ ,  $q_r = 0.01$ ) patterns emerge behind the Fisher-like front for all values of  $\mu$ . This is consistent with the linear stability analysis — see Fig. 2(d). For small values of  $\mu$ ,  $\mu = 0.1$  and  $\mu = 0.3$  in Figs. 6(a) and 6(b), respectively, the cancer cells exhibit merging and emerging peaks; cells move towards each other forming new aggregations of new cells and of cells that broke off from existing aggregations and in the long-term dynamics stationary pulses are also formed. (Bitsouni et al, 2017; Loy and Preziosi, 2019; Eftimie et al, 2017; Wang and Hillen, 2007). For larger values of  $\mu$ , and consequently larger values of  $\text{Ca}^{2+}$  (see Figs. 6(c) and 6(d)) the patterns are thin stripes (stationary pulses).

In Figs. 5 and 6 attraction dominates over repulsion. In Fig. 7 we plot the cancer cell density when repulsion is stronger than attraction ( $q_a = 0.14$ ,  $q_r = 0.22$ ). For small values of the  $\text{InsP}_3$  concentration ( $\mu = 0.1$ ,  $\mu = 0.3$ ), Figs. 7(a),(b) exhibit thin-stripe patterns via ADI (stationary pulses). As we increase  $\mu$ , patterns vanish — see Figs. 7(c) and 7(d), respectively for  $\mu = 0.45$  and  $\mu = 0.6$ . These results are consistent with Fig. 2(f). Finally, for large and equal values of  $q_a$  and  $q_r$ , Figs. 2(g) and 2(h) predict that ADI patterns exist for all  $\text{Ca}^{2+}$  concentrations within the physiological range of the Atri model. This is confirmed in Fig. 8, where we observe ADI patterns for any  $\text{InsP}_3$  (and  $\text{Ca}^{2+}$ ) level when  $q_a = q_r = 0.33$ .

Above, we have established the emergence and disappearance of patterns as  $\text{Ca}^{2+}$  varies. Furthermore, below we will summarise the effect of  $\text{Ca}^{2+}$  on three important characteristics of the solution: the wave speed of the Fisher-like front, and also the amplitude and frequency of the cancer cell density.

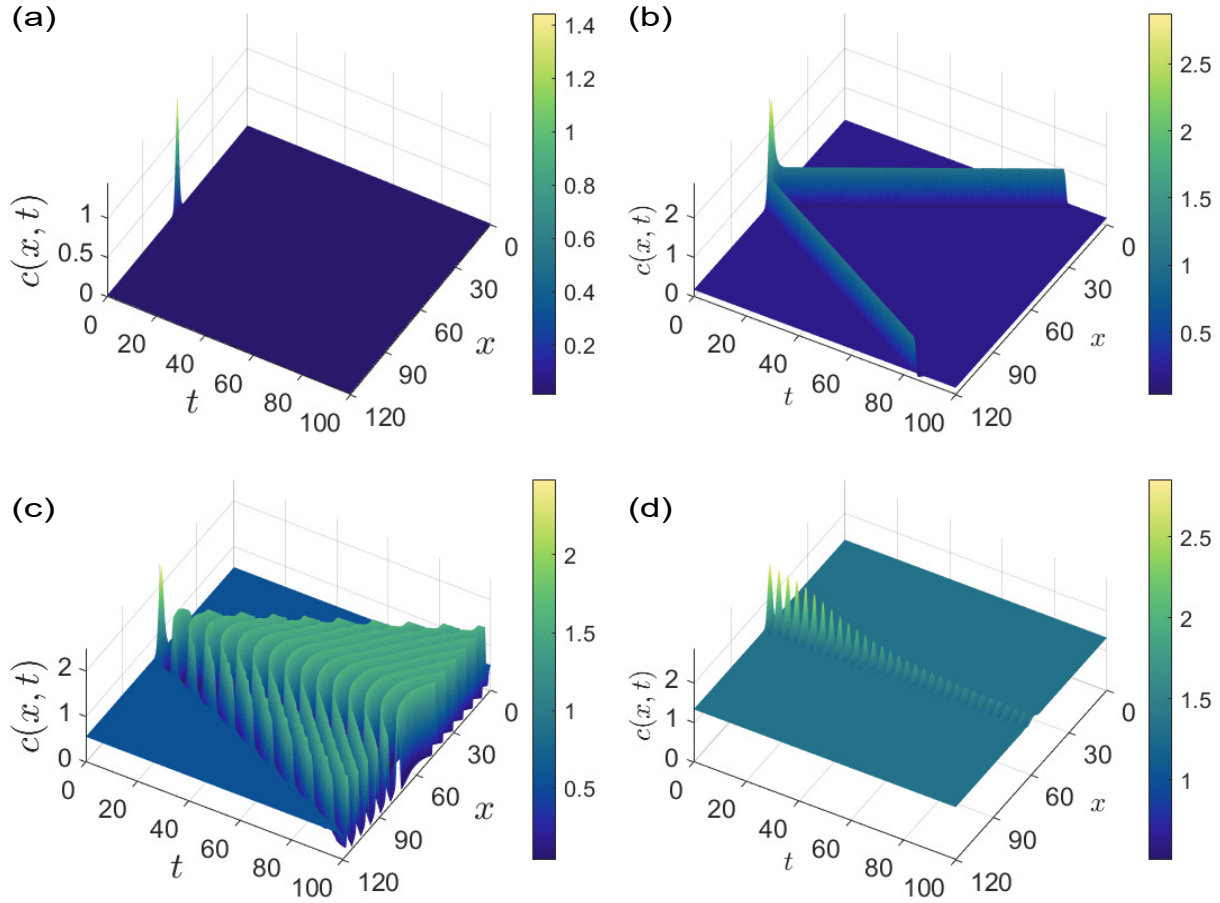


Fig. 4: Patterns of the  $\text{Ca}^{2+}$  concentration,  $c(x, t)$ , generated by the Atri model (2.7a)-(2.7b) for (a)  $\mu = 0.1$  ( $c^* = 0.016$ ), (b)  $\mu = 0.288$  ( $c^* = 0.177$ ), (c)  $\mu = 0.3$  and (d)  $\mu = 0.5$  ( $c^* = 1.332$ ). The initial conditions are given in (4.1a)-(4.1b). The remaining parameter values are given in Tables 1 and 2. Note that although we report  $c^*$  for all  $\mu$  when  $\text{Ca}^{2+}$  is oscillatory the steady state is linearly unstable

*Wave speed:* In Figs. 5–8 we see that as  $\mu$  increases (fixed  $q_a$  and  $q_r$ ) the speed of the travelling front increases. This can be linked to a higher invasion and hence metastatic potential of the cancer cells. On the other hand, for fixed  $\mu$  the wave speed does not change much as  $q_a$  and/or  $q_r$  vary.

*Amplitude:* Comparing Figs. 5 and 6 we see that the maximal cell density increases as  $q_a$ , the attraction magnitude, increases from 0.14 to 0.33. Also, comparing Figs. 6 and 8 we see a significant increase in the maximal cell density as  $q_r$  increases from 0.01 to 0.33 (and  $q_a$  fixed to 0.33). The same effect is observed when comparing Fig. 5-top panel with Fig. 7, where again  $q_r$  increases from 0.01 to 0.33 (while  $q_a$  is fixed to 0.14). For fixed  $q_a$  and  $q_r$  as  $\mu$  increases the maximal cell density decreases, as we can see in Figs. 5–8.

*Frequency:* Moreover, we investigate how  $\text{Ca}^{2+}$  signalling affects the temporal frequency of cancer cell density oscillations. In Fig. 9 we fix  $x = 55$  and plot  $c(x, t)$  and  $u(x, t)$  for two choices; at the top panel we have  $q_a = 0.22$ ,  $q_r = 0.01$  (attraction much larger than repulsion) and in the bottom panel we have  $q_a = 0.14$ ,  $q_r = 0.22$  (attraction comparable to repulsion). From the frequency bifurcation diagram of the Atri model



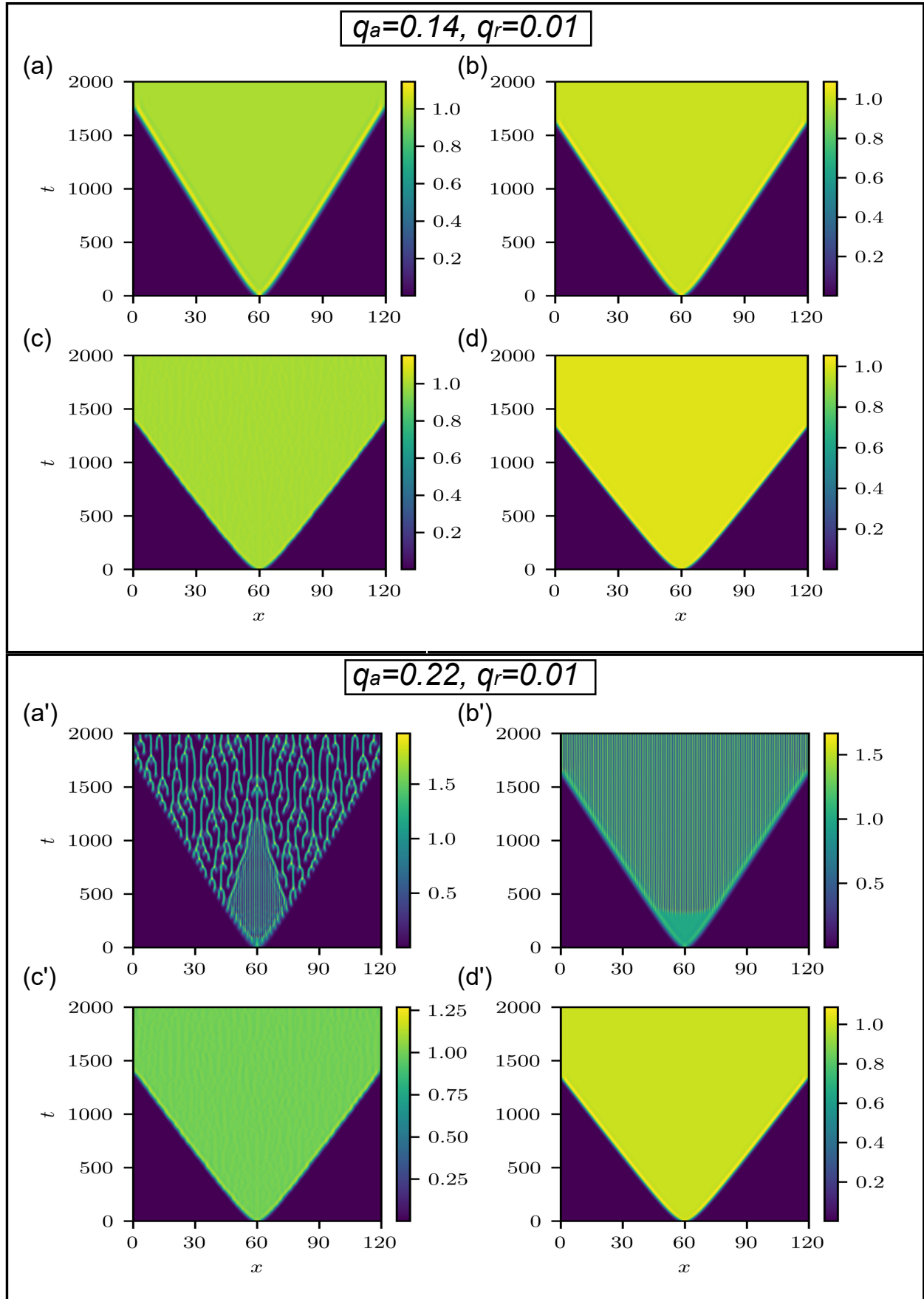


Fig. 5: Cancer cell density,  $u(x, t)$ , governed by equation (2.7c), as  $q_a$  increases (top panel for  $q_a = 0.14$  and bottom panel for  $q_a = 0.22$ );  $q_r = 0.01$ . The initial conditions are given by (4.1). For (a), (a')  $\mu = 0.1$ ,  $c^* = 0.016$  (non-oscillatory  $\text{Ca}^{2+}$ ); (b), (b')  $\mu = 0.1$ ,  $c^* = 0.016$  (oscillatory  $\text{Ca}^{2+}$ ); (c), (c')  $\mu = 0.1$ ,  $c^* = 0.016$  (oscillatory  $\text{Ca}^{2+}$ ); (d), (d')  $\mu = 0.1$ ,  $c^* = 0.016$  (oscillatory  $\text{Ca}^{2+}$ ).

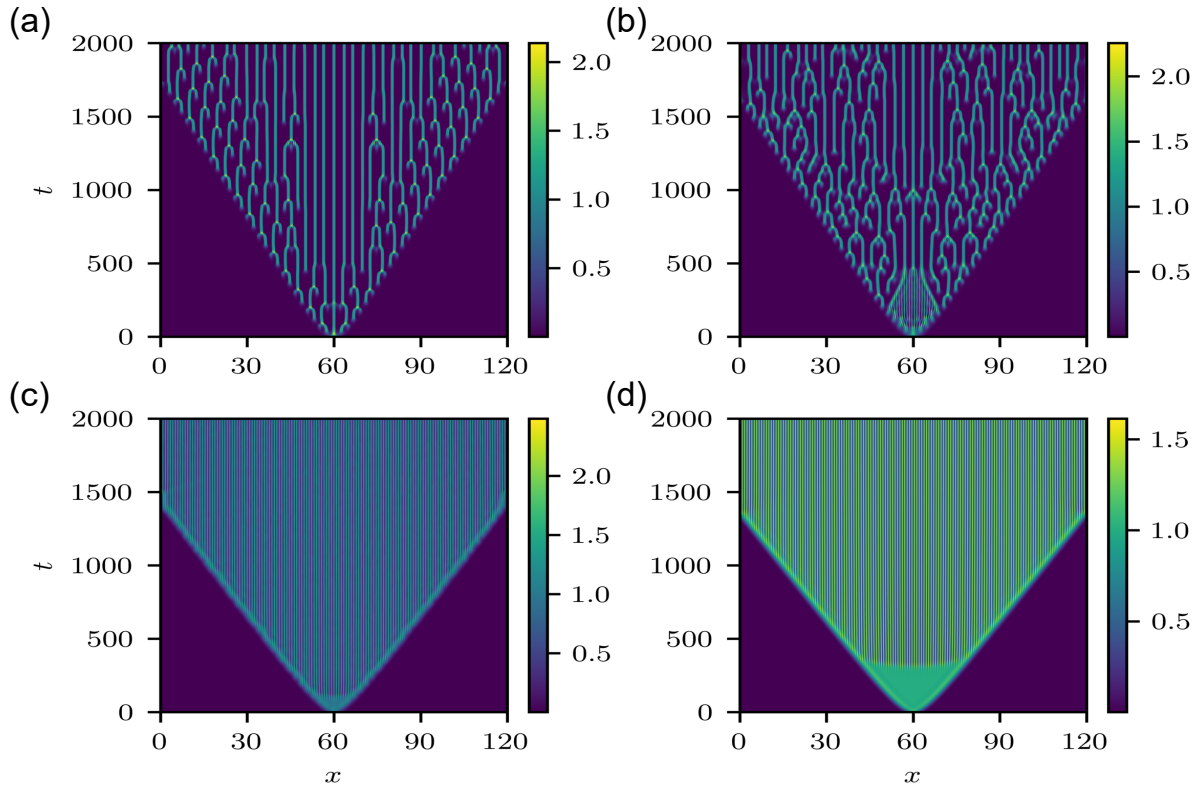


Fig. 6: Cancer cell density,  $u(x,t)$ , governed by equation (2.7c), for  $q_a = 0.33$ ,  $q_r = 0.01$ . The initial conditions are given in (4.1). (a)  $\mu = 0.1$ ,  $c^* = 0.016$  (non-oscillatory  $\text{Ca}^{2+}$ ); (b)  $\mu = 0.3$ ,  $c^* = 0.556$  (oscillatory  $\text{Ca}^{2+}$ ); (c)  $\mu = 0.45$ ,  $c^* = 1.195$  (oscillatory  $\text{Ca}^{2+}$ ); (d)  $\mu = 0.6$ ,  $c^* = 1.5712$  (non-oscillatory  $\text{Ca}^{2+}$ ). The rest of model parameters are given in Tables 1 and 2. Note that although we report  $c^*$  for all  $\mu$  when  $\text{Ca}^{2+}$  is oscillatory the steady state is linearly unstable.

(see Fig. 2 in Kaouri et al (2019)) we choose four values of  $\mu$  that sufficiently ‘sample’ the variation of the frequency as  $\mu$  increases. We see that the frequency of  $\text{Ca}^{2+}$  oscillations is approximately equal to the frequency of cell density oscillations, **if** the cell density is oscillatory. We have verified this observation by also computing the frequency spectra for  $t \in (1900, 2000)$  (the time interval has been chosen to ensure that solutions converged to steady state). For other choices of  $q_a$  and  $q_r$ , the effect of  $\text{Ca}^{2+}$  oscillations on the cell density is similar, and thus other figures are not included for brevity.

## 5 Summary, conclusions and further work

Since cell proliferation and cell-cell adhesion, which play a critical role in invasion and cancer metastasis, are  $\text{Ca}^{2+}$ -dependent, here we have developed and analysed a new model for  $\text{Ca}^{2+}$  signalling in cancer. The  $\text{Ca}^{2+}$  dynamics have been described by the spatially extended Atri model (Atri et al, 1993), which consists of a reaction-diffusion equation for the  $\text{Ca}^{2+}$  concentration, coupled with an ODE for the fraction of  $\text{InsP}_3$  receptors on the ER that have not been inactivated by  $\text{Ca}^{2+}$ . This model, although simple enough, generates

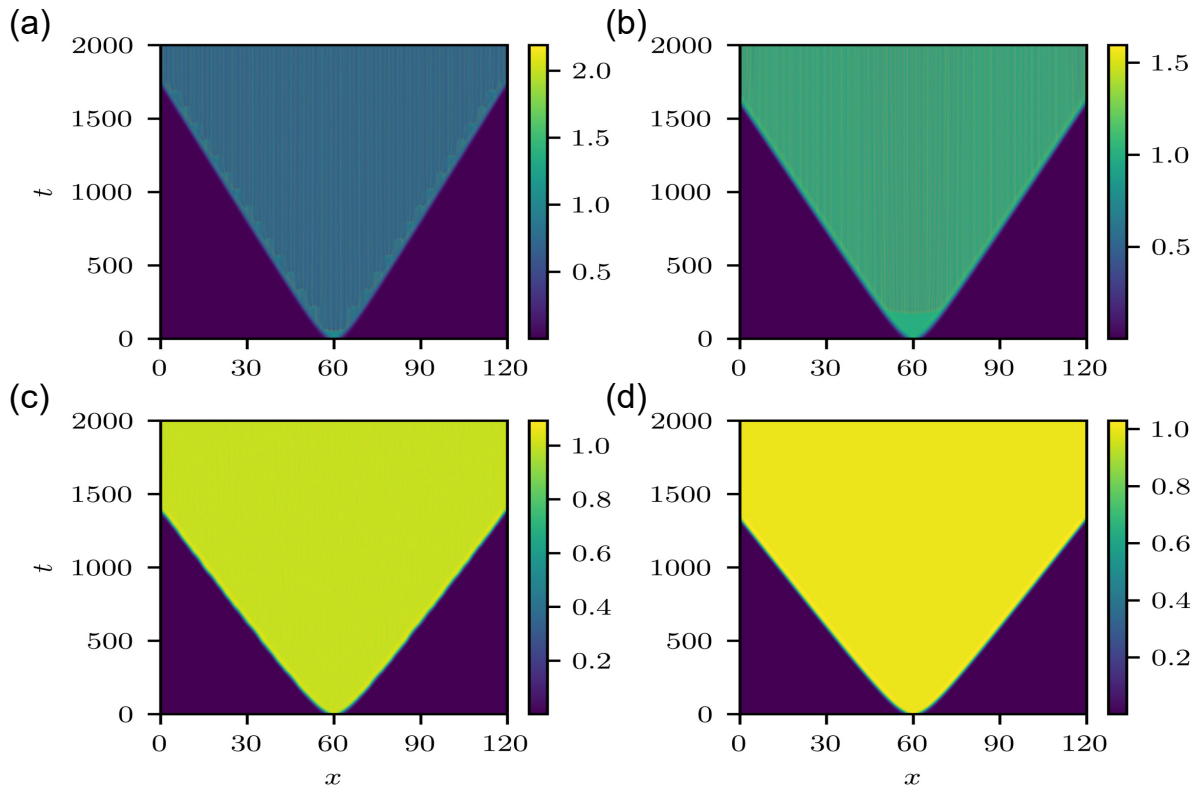


Fig. 7: Cancer cell density,  $u(x, t)$ , governed by equation (2.7c), for  $q_a = 0.14$  and  $q_r = 0.22$ . The initial conditions are given in (4.1). (a)  $\mu = 0.1$ ,  $c^* = 0.016$  (non-oscillatory  $\text{Ca}^{2+}$ ); (b)  $\mu = 0.3$ ,  $c^* = 0.556$  (oscillatory  $\text{Ca}^{2+}$ ); (c)  $\mu = 0.45$ ,  $c^* = 1.195$  (oscillatory  $\text{Ca}^{2+}$ ); (d)  $\mu = 0.6$ ,  $c^* = 1.5712$  (non-oscillatory  $\text{Ca}^{2+}$ ). The rest of model parameters are given in Tables 1 and 2. Note that although we report  $c^*$  for all  $\mu$  when  $\text{Ca}^{2+}$  is oscillatory the steady state is linearly unstable.

four ‘prototypical’  $\text{Ca}^{2+}$  signals as many other excitable  $\text{Ca}^{2+}$  models; periodic wavetrains (which correspond to limit cycles in the spatially clamped Atri model), solitary pulses (which correspond to action potentials), decaying wavetrains and solutions decreasing monotonically with time. The cancer cell density evolution is described by a non-local PDE that incorporates diffusion, cell-cell adhesion (advection) and proliferation. We have modelled the dependence of the adhesion and proliferation terms on the  $\text{Ca}^{2+}$  dynamics, motivated by experimental evidence, and we have considered cancer types where the adhesion strength decreases with  $\text{Ca}^{2+}$  (Byers et al, 1995; Cavallaro and Christofori, 2004), while proliferation increases with  $\text{Ca}^{2+}$  (Cárdenas et al, 2016; Prevarskaya et al, 2018; Rezuchova et al, 2019; Tsunoda et al, 2005). The model, assumptions and parameter values are presented in Section 2. As much as possible, the model parameters were chosen from experimental studies (see Tables 1 and 2).

In Section 3 we linearised the model (2.7) and determined the parameter range for which an adhesion-driven instability (ADI) forms, while varying systematically the magnitudes of cell-cell attraction and repulsion,  $q_a$  and  $q_r$ , respectively. In the absence of  $\text{Ca}^{2+}$  (Fig. 1) we showed that ADIs may arise for sufficiently large values of either  $q_a$  and  $q_r$  (or both). ADIs correspond to cell aggregations which are critical for cancer

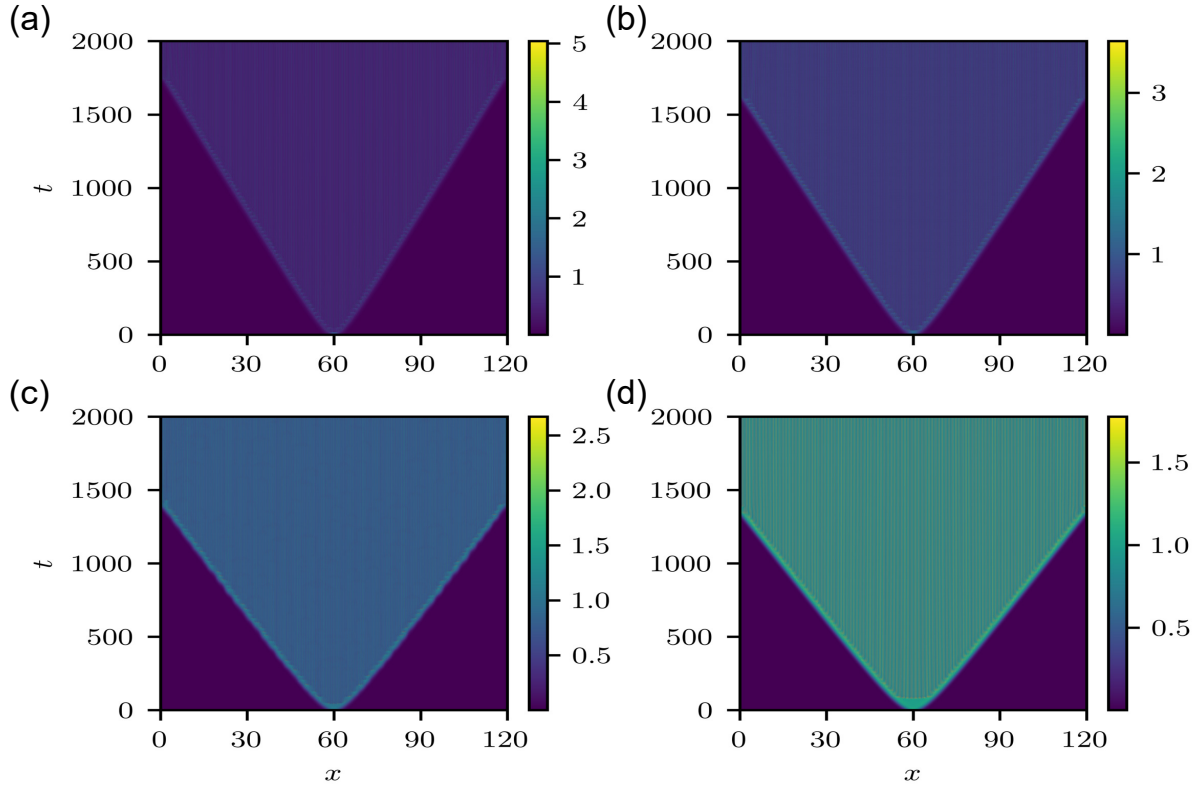
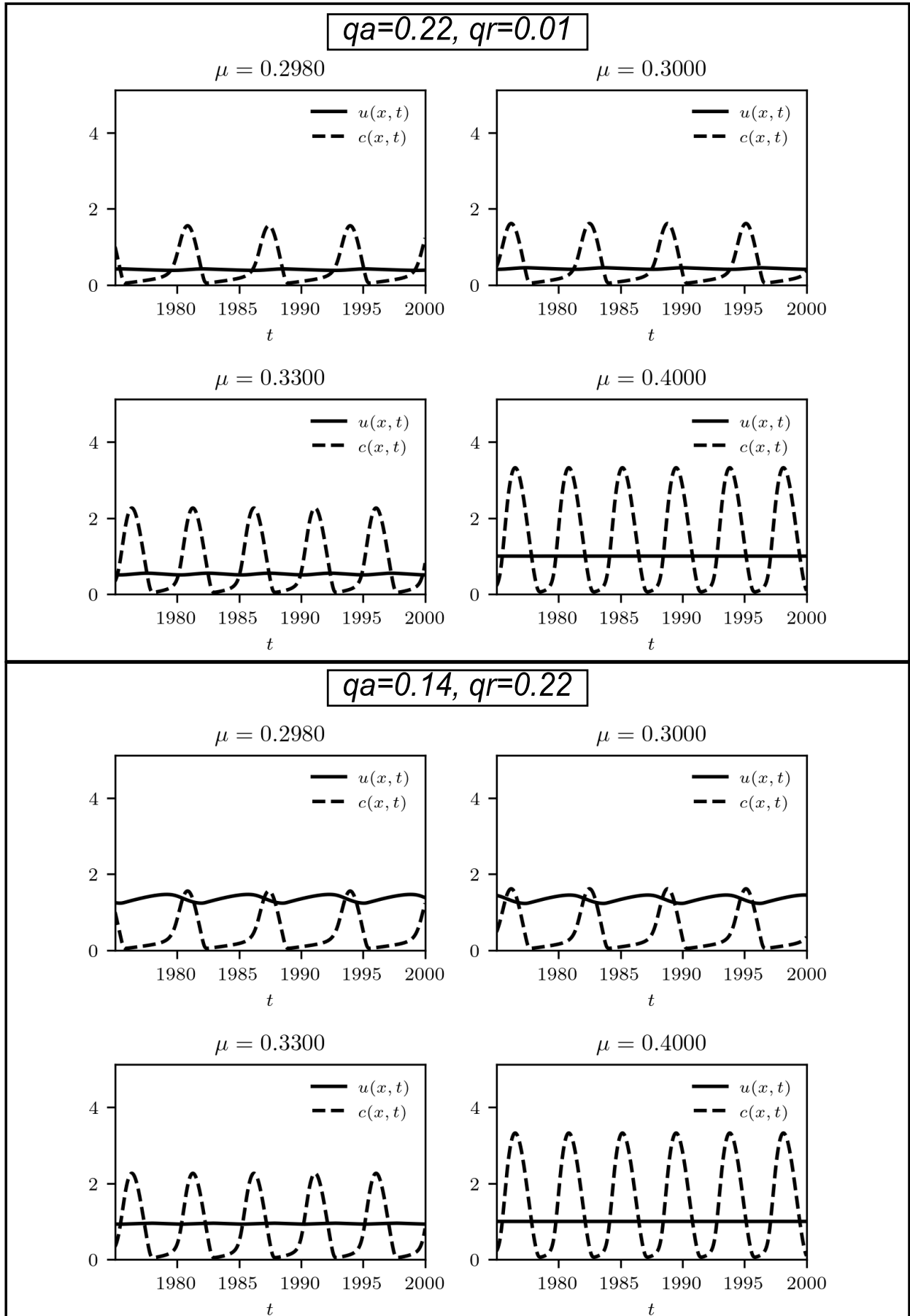


Fig. 8: Cancer cell density,  $u(x, t)$ , governed by equation (2.7c), for  $q_a = q_r = 0.33$ . The initial conditions are given in (4.1). (a)  $\mu = 0.1$ ,  $c^* = 0.016$  (non-oscillatory  $\text{Ca}^{2+}$ ); (b)  $\mu = 0.3$ ,  $c^* = 0.556$  (oscillatory  $\text{Ca}^{2+}$ ); (c)  $\mu = 0.45$ ,  $c^* = 1.195$  (oscillatory  $\text{Ca}^{2+}$ ); (d)  $\mu = 0.6$ ,  $c^* = 1.5712$  (non-oscillatory  $\text{Ca}^{2+}$ ). The rest of model parameters are given in Tables 1 and 2. The results are consistent with Fig. 2(g). Note that although we report  $c^*$  for all  $\mu$  when  $\text{Ca}^{2+}$  is oscillatory the steady state is linearly unstable.

invasion and metastasis. Then, in Fig. 2 we investigated the effect of  $\text{Ca}^{2+}$  on the cell aggregations and found that they change qualitatively and eventually vanish as the  $\text{Ca}^{2+}$  level increases.

In Section 4 we solved the full non-linear model (2.7) numerically and systematically investigated a range of attraction and repulsion magnitudes, guided by the linear stability analysis. Firstly, we validated numerically the results of the linear analysis in the absence of  $\text{Ca}^{2+}$  (Fig. 3). We subsequently examined the effect of four types of  $\text{Ca}^{2+}$  signals on the cancer cell density, paying special attention to the periodic wave trains (Figs. 5-8). We found that as  $\text{Ca}^{2+}$  levels increase the maximal cell density decreases due to the decreased cell-cell adhesion strength preventing the formation of clusters of high density levels. Moreover, as  $\text{Ca}^{2+}$  levels increase the speed of the travelling wave fronts increases which is linked to a faster spread of cancer. An other important result from our numerical investigations is that the frequency of  $\text{Ca}^{2+}$  oscillations is approximately equal to the frequency of the cancer cell density oscillations, when the cell density is oscillatory. Moreover, cellular aggregations vanish for sufficiently large  $\text{Ca}^{2+}$  levels, as it was predicted by the linear analysis. Our results demonstrate that accounting for the dependence of cell-cell adhesion and proliferation on  $\text{Ca}^{2+}$  signalling we can reveal the conditions for which cancer cell aggregations appear as



$\text{Ca}^{2+}$  varies. This allows us to study the dependence of the cancer invasion potential on  $\text{Ca}^{2+}$  and paves the ways for new therapies based on controlling  $\text{Ca}^{2+}$ .

Our model provides a general framework for cancer cell movement under the effect of any oscillatory signalling pathway dynamics and paves the way for treatments that are based on controlling these pathways, and in particular  $\text{Ca}^{2+}$  signalling. It, however, has various limitations which outline avenues for future work. The assumption that the adhesion strength function is decreasing with  $\text{Ca}^{2+}$  is not appropriate for all cancer types; an increase of cell-cell adhesion with  $\text{Ca}^{2+}$  has been observed in some cancers. Additionally, the repulsion magnitude has been taken over a wide range since there is no experimental evidence supporting its value. New experiments could investigate this. Another limitation of the model is that it includes cell-cell interactions; it would be useful to incorporate the interaction of the cancer cells with the extracellular matrix (ECM) in future work as this would allow to study cancer invasion in more detail. Additionally, the way cell-ECM interactions are dependent on  $\text{Ca}^{2+}$  could be also modelled. Finally, the delay of the  $\text{Ca}^{2+}$  waves in the gap junctions between cells has been considered negligible; a cell-based model accounting for these gap junctions could be developed. Moreover, as we are now equipped with the insights generated by the one-dimensional geometry, we plan to develop the model to two and three dimensions.

A main focus of this study was to unravel the impact of the cellular  $\text{Ca}^{2+}$  signalling on the behaviour of cancer cells. As such, a key component of our model is the description of the cellular  $\text{Ca}^{2+}$  dynamics. We chose the Atri model as a typical representative for a minimal framework that captures essential features of the dynamics of the cellular  $\text{Ca}^{2+}$  concentration such as  $\text{Ca}^{2+}$  oscillations. This naturally raises the question about how robust our results are with respect to the  $\text{Ca}^{2+}$  model that we employed. The answer to this question combines two main lines of argument: the specific model for the  $\text{InsP}_3\text{R}$  and whether  $\text{Ca}^{2+}$  oscillations are deterministic or stochastic. For the first point, we note that there exist a substantial number of  $\text{InsP}_3\text{R}$  models, see e.g. (Atri et al, 1993; De Young and Keizer, 1992; Li et al, 1994; Li and Rinzel, 1994b; Meyer and Stryer, 1988; Sneyd and Dufour, 2002; Siekmann et al, 2012; Sneyd and Falcke, 2005; Shuai et al, 2007; Ullah et al, 2012). While they differ in their complexity, the overall range of the  $\text{Ca}^{2+}$  concentration and the frequency of the  $\text{Ca}^{2+}$  oscillations are comparable amongst them. Consequentially, exchanging the Atri model for any of the other  $\text{InsP}_3\text{R}$  models will most probably not change our conclusions. A more contentious point is whether  $\text{Ca}^{2+}$  oscillations should be described within a deterministic or stochastic framework. Both approaches have been used extensively to date as e.g. in (Dupont et al, 2011b; Falcke et al, 2018; Gaspers et al, 2014; Kummer et al, 2000; Li and Rinzel, 1994a; Politi et al, 2006; Powell et al, 2020; Shuai and Jung, 2002; Skupin et al, 2008; Sneyd et al, 2017; Sun et al, 2017; Tang et al, 1996; Thul et al, 2009; Thul and Falcke, 2007, 2006, 2004a,b; Thurley et al, 2011; Tilunaite et al, 2017; Thul, 2014; Thurley et al, 2012; Tsaneva-Atanasova et al, 2005; Voorsluijs et al, 2019; Weinberg and Smith, 2014; Wieder et al, 2015) — see also the book by (Dupont et al, 2016b) for a detailed discussion. As this study is the first to explore the role of  $\text{Ca}^{2+}$  in a mathematical model of cancer cell propagation, we opted for a deterministic approach. This provides us with a baseline against which we can test future models in which the  $\text{Ca}^{2+}$  dynamics will be described stochastically.

**Acknowledgements** The authors would like to thank Dr. A. Athenodorou for his valuable technical support. VB acknowledges support from the European Union's H2020 Research and Innovation Action under Grant Agreement No 741657 (SciShops.eu). AB was partially supported by an NSERC (Natural Sciences and Engineering Research Council) post-doctoral fellowship, and is grateful to the Pacific Institute for Mathematical Sciences for providing space and resources for AB's postdoctoral research.

## References

- Alberts B, Lewis J, Bray D (2000) Molecular biology of the cell. Garland Science  
 Allbritton NL, Meyer T, Stryer L (1992) Range of messenger action of calcium ion and inositol 1, 4, 5-trisphosphate. *Science* 258(5089):1812–1815

- Andasari V, Gerisch A, Lolas G, South AP, Chaplain MA (2011) Mathematical modeling of cancer cell invasion of tissue: biological insight from mathematical analysis and computational simulation. *J Math Biol* 63(1):141–171
- Armstrong NJ, Painter KJ, Sherratt JA (2006) A continuum approach to modelling cell–cell adhesion. *J Theor Biol* 243(1):98–113
- Atri A, Amundson J, Clapham D, Sneyd J (1993) A single-pool model for intracellular calcium oscillations and waves in the xenopus laevis oocyte. *Biophys J* 65(4):1727–1739
- Bereiter-Hahn J (2005) Mechanics of crawling cells. *Med Eng Phys* 27(9):743–753
- Berridge MJ, Galione A (1988) Cytosolic Calcium Oscillators. *The FASEB Journal* 2(15):3074–3082
- Berridge MJ, Lipp P, Bootman MD (2000) The versatility and universality of calcium signalling. *Nature Reviews Molecular Cell Biology* 1(1):11–21
- Bitsouni V, Eftimie R (2018) Non-local parabolic and hyperbolic models for cell polarisation in heterogeneous cancer cell populations. *Bull Math Biol* 80(10):2600–2632
- Bitsouni V, Chaplain MA, Eftimie R (2017) Mathematical modelling of cancer invasion: the multiple roles of TGF- $\beta$  pathway on tumour proliferation and cell adhesion. *Math Mod Meth Appl S* 27(10):1929–1962
- Bitsouni V, Trucu D, Chaplain MA, Eftimie R (2018) Aggregation and travelling wave dynamics in a two-population model of cancer cell growth and invasion. *Math Med Biol* 35(4):541–577
- Boulter E, Grall D, Cagnol S, Van Obberghen-Schilling E, Boulter E, Grall D, Cagnol S, Van Obberghen-Schilling E (2006) Regulation of cell-matrix adhesion dynamics and rac-1 by integrin linked kinase. *Faseb J* 20(9):1489–1491
- Bray D (1992) *Cell movements* garland publishing. Inc, New York
- Byers SW, Sommers CL, Hoxter B, Mercurio AM, Tozeren A (1995) Role of E-cadherin in the response of tumor cell aggregates to lymphatic, venous and arterial flow: measurement of cell-cell adhesion strength. *J Cell Sci* 108(5):2053–2064
- Capiod T, Shuba Y, Skryma R, Prevarskaya N (2007) Calcium signalling and cancer cell growth. In: *Calcium Signalling and Disease*, Springer, pp 405–427
- Cárdenas C, Müller M, McNeal A, Lovy A, Jaña F, Bustos G, Urrea F, Smith N, Molgó J, Diehl JA, et al (2016) Selective vulnerability of cancer cells by inhibition of Ca<sup>2+</sup> transfer from endoplasmic reticulum to mitochondria. *Cell Reports* 14(10):2313–2324
- Cavallaro U, Christofori G (2001) Cell adhesion in tumor invasion and metastasis: loss of the glue is not enough. *BBA-Rev Cancer* 1552(1):39–45
- Cavallaro U, Christofori G (2004) Cell adhesion and signalling by cadherins and Ig-CAMs in cancer. *Nat Rev Canc* 4(2):118
- Cavallaro U, Schaffhauser B, Christofori G (2002) Cadherins and the tumour progression: is it all in a switch? *Cancer Letters* 176(2):123–128
- Chaplain MA, Lolas G (2006) Mathematical modelling of cancer invasion of tissue: dynamic heterogeneity. *NHM* 1(3):399–439
- Chaplain MA, Lachowicz M, Szymańska Z, Wrzosek D (2011) Mathematical modelling of cancer invasion: the importance of cell–cell adhesion and cell–matrix adhesion. *Math Mod Meth Appl S* 21(04):719–743
- Charles AC, Merrill JE, Dirksen ER, Sandersont MJ (1991) Intercellular signaling in glial cells: calcium waves and oscillations in response to mechanical stimulation and glutamate. *Neuron* 6(6):983–992
- Charles AC, Naus C, Zhu D, Kidder GM, Dirksen ER, Sanderson MJ (1992) Intercellular calcium signaling via gap junctions in glioma cells. *J Cell Biol* 118(1):195–201
- Charles AC, Dirksen ER, Merrill JE, Sanderson MJ (1993) Mechanisms of intercellular calcium signaling in glial cells studied with dantrolene and thapsigargin. *Glia* 7(2):134–145
- Clark AG, Vignjevic DM (2015) Modes of cancer cell invasion and the role of the microenvironment. *Curr Opin Cell Biol* 36:13–22
- Colomer J, Means A (2007) Physiological roles of the Ca<sup>2+</sup>/CaM-dependent protein kinase cascade in health and disease. In: *Calcium Signalling and Disease*, Springer, pp 169–214

- Cunningham D, You Z (2015) In vitro and in vivo model systems used in prostate cancer research. *J Biol Meth* 2(1)
- De Young GW, Keizer J (1992) A single-pool inositol 1, 4, 5-trisphosphate-receptor-based model for agonist-stimulated oscillations in  $\text{Ca}^{2+}$  concentration. *Proc Natl Acad Sci Unit States Am* 89(20):9895–9899
- Deguchi R, Shirakawa H, Oda S, Mohri T, Miyazaki S (2000) Spatiotemporal analysis of  $\text{Ca}^{2+}$  waves in relation to the sperm entry site and animal-vegetal axis during  $\text{Ca}^{2+}$  oscillations in fertilized mouse eggs. *Developmental biology* 218(2):299–313
- Domschke P, Trucu D, Gerisch A, Chaplain MA (2014) Mathematical modelling of cancer invasion: implications of cell adhesion variability for tumour infiltrative growth patterns. *J Theor Biol* 361:41–60
- Dupont G, Combettes L (2016) Fine tuning of cytosolic  $\text{Ca}^{2+}$  oscillations. *F1000Research* 5(2036)
- Dupont G, Combettes L, Bird GS, Putney JW (2011a) Calcium oscillations. *Cold Spring Harbor Perspectives in Biology* 3(3):pii: a004,226
- Dupont G, Lokenye EFL, Challiss RAJ (2011b) A model for  $\text{Ca}^{2+}$  oscillations stimulated by the type 5 metabotropic glutamate receptor: an unusual mechanism based on repetitive, reversible phosphorylation of the receptor. *Biochimie* 93(12):2132–2138
- Dupont G, Falcke M, Kirk V, Sneyd J (2016a) *Models of Calcium Signalling, Interdisciplinary Applied Mathematics*, vol 43. Springer
- Dupont G, Falcke M, Kirk V, Sneyd J (2016b) *Models of calcium signalling*, vol 43. Springer
- Dyson R, Green J, Whiteley J, Byrne H (2016) An investigation of the influence of extracellular matrix anisotropy and cell-matrix interactions on tissue architecture. *J Math Biol* 72:1775–1809, DOI 10.1007/s00285-015-0927-7
- Eftimie R, de Vries G, Lewis M, Lutscher F (2007) Modeling group formation and activity patterns in self-organizing collectives of individuals. *Bull Math Biol* 69(5):1537–1565
- Eftimie R, Perez M, Buono PL (2017) Pattern formation in a nonlocal mathematical model for the multiple roles of the TGF- $\beta$  pathway in tumour dynamics. *Math Biosci* 289:96–115
- Enderling H, Anderson AR, Chaplain MA, Munro AJ, Vaidya JS (2006) Mathematical modelling of radiotherapy strategies for early breast cancer. *J Theor Biol* 241(1):158–171
- Engwer C, Stinner C, Surulescu C (2017) On a structured multiscale model for acid-mediated tumor invasion: The effects of adhesion and proliferation. *Mathematical Models and Methods in Applied Sciences* 27(07):1355–1390
- Estrada J, Andrew N, Gibson D, Chang F, Gnad F, Gunawardena J (2016) Cellular interrogation: exploiting cell-to-cell variability to discriminate regulatory mechanisms in oscillatory signalling. *PLoS computational biology* 12(7):e1004,995
- Falcke M, Moein M, Tilunait A, Thul R, Skupin A (2018) On the phase space structure of  $\text{IP}_3$  induced  $\text{Ca}^{2+}$  signalling and concepts for predictive modeling. *Chaos* 28(4):045,115
- Franssen LC, Lorenzi T, Burgess AE, Chaplain MA (2019) A mathematical framework for modelling the metastatic spread of cancer. *Bull Math Biol* 81(6):1965–2010
- Friedl P, Hegerfeldt Y, Tusch M (2004) Collective cell migration in morphogenesis and cancer. *International Journal of Developmental Biology* 48(5-6):441–449
- Gaspers LD, Bartlett PJ, Politi A, Burnett P, Metzger W, Johnston J, Joseph SK, Höfer T, Thomas J (2014) Hormone-induced calcium oscillations depend on cross-coupling with inositol 1,4,5-trisphosphate oscillations. *Cell Reports* 9(4):1209–1218
- Gerisch A (2001) Numerical methods for the simulation of taxis-diffusion-reaction systems. PhD thesis, Ph. D. thesis, Martin-Luther-Universität Halle-Wittenberg, Germany
- Gerisch A (2010) On the approximation and efficient evaluation of integral terms in pde models of cell adhesion. *IMA journal of numerical analysis* 30(1):173–194
- Gerisch A, Chaplain M (2008) Mathematical modelling of cancer cell invasion of tissue: local and non-local models and the effect of adhesion. *J Theor Biol* 250(4):684–704



- Gerisch A, Painter KJ (2010) Mathematical modelling of cell adhesion and its applications to developmental biology and cancer invasion. *Cell mechanics: from single scale-based models to multiscale modeling* 2:319–350
- Glinsky VV, Glinsky GV, Glinskii OV, Huxley VH, Turk JR, Mossine VV, Deutscher SL, Pienta KJ, Quinn TP (2003) Intravascular metastatic cancer cell homotypic aggregation at the sites of primary attachment to the endothelium. *Cancer research* 63(13):3805–3811
- Goswami S, Sahai E, Wyckoff JB, Cammer M, Cox D, Pixley FJ, Stanley ER, Segall JE, Condeelis JS (2005) Macrophages promote the invasion of breast carcinoma cells via a colony-stimulating factor-1/epidermal growth factor paracrine loop. *Cancer Res* 65(12):5278–5283
- Green J, Waters S, Whiteley J, Edelstein-Keshet L, Shakesheff K, Byrne H (2010) Non-local models for the formation of hepatocyte–stellate cell aggregates. *J Theor Biol* 267(1):106–120
- Ha CE, Bhagavan N (2011) *Essentials of medical biochemistry: With clinical cases*. Academic Press
- Hagemann T, Wilson J, Kulbe H, Li NF, Leinster DA, Charles K, Klemm F, Pukrop T, Binder C, Balkwill FR (2005) Macrophages induce invasiveness of epithelial cancer cells via NF- $\kappa$ B and JNK. *J Immunol* 175(2):1197–1205
- Henry D (1981) *Geometric theory of semilinear parabolic systems*, vol 840. Springer-Verlag
- Hillen T, Buttenschön A (2019) Nonlocal adhesion models for microorganisms on bounded domains. arXiv preprint arXiv:190306635
- Hillen T, Painter KJ (2009) A user’s guide to pde models for chemotaxis. *J Math Biol* 58(1-2):183
- Hills CE, Younis MY, Bennett J, Siamantouras E, Liu KK, Squires PE (2012) Calcium-sensing receptor activation increases cell-cell adhesion and  $\beta$ -cell function. *Cell Physiol Biochem* 30(3):575–586
- Höfer T, Politi A, Heinrich R (2001) Intercellular  $\text{Ca}^{2+}$  wave propagation through gap-junctional  $\text{Ca}^{2+}$  diffusion: a theoretical study. *Biophys J* 80(1):75–87
- Hundsdoerfer W, Verwer JG (2003) *Numerical solution of time-dependent advection-diffusion-reaction equations*, vol 33. Springer Science & Business Media
- Kaouri K, Maini PK, Skourides P, Christodoulou N, Chapman SJ (2019) A simple mechanochemical model for calcium signalling in embryonic epithelial cells. *J Math Biol* 78(7):2059–2092
- Keener J, Sneyd J (2009a) *Mathematical physiology I: Cellular physiology*, vol 2. Springer
- Keener J, Sneyd J (2009b) *Mathematical physiology II: Systems Physiology*, vol 2. Springer
- Keller EF, Segel LA (1970) Initiation of slime mold aggregation viewed as an instability. *J Theor Biol* 26(3):399–415
- Kim SA, Tai CY, Mok LP, Mosser EA, Schuman EM (2011) Calcium-dependent dynamics of cadherin interactions at cell–cell junctions. *Proceedings of the National Academy of Sciences* 108(24):9857–9862
- Knútsdóttir H, Pálsson E, Edelstein-Keshet L (2014) Mathematical model of macrophage-facilitated breast cancer cells invasion. *J Theor Biol* 357:184–199
- Ko KS, Arora PD, Bhide V, Chen A, McCulloch C (2001) Cell-cell adhesion in human fibroblasts requires calcium signaling. *J Cell Sci* 114(6):1155–1167
- Kotteas EA, Boulas P, Gkiozos I, Tsagkouli S, Tsoukalas G, Syrigos KN (2014) The intercellular cell adhesion molecule-1 (icam-1) in lung cancer: implications for disease progression and prognosis. *Anticancer research* 34(9):4665–4672
- Kummer U, Olsen LF, Dixon CJ, Green AK, Bornberg-Bauer E, Baier G (2000) Switching from simple to complex oscillations in calcium signaling. *Biophysical Journal* 79(3):1188–1195
- Laird AK (1964) Dynamics of tumour growth. *Brit J Cancer* 18(3):490
- Li Y, Rinzel J (1994a) Equations for  $\text{InsP}_3$  receptor-mediated  $[\text{Ca}^{2+}]_i$  oscillations derived from a detailed kinetic model: a Hodgkin-Huxley like formalism. *J Theor Biol* 166(4):461–473
- Li YX, Rinzel J (1994b) Equations for  $\text{InsP}_3$  receptor-mediated  $[\text{Ca}^{2+}]_i$  oscillations derived from a detailed kinetic model: a hodgkin-huxley like formalism. *J Theor Biol* 166(4):461–473
- Li YX, Rinzel J, Keizer J, Stojilković SS (1994) Calcium oscillations in pituitary gonadotrophs: comparison of experiment and theory. *Proc Natl Acad Sci Unit States Am* 91(1):58–62

- Lin EY, Li JF, Gnatovskiy L, Deng Y, Zhu L, Grzesik DA, Qian H, Xue Xn, Pollard JW (2006) Macrophages regulate the angiogenic switch in a mouse model of breast cancer. *Cancer Res* 66(23):11,238–11,246
- Loy N, Preziosi L (2019) Modelling physical limits of migration by a kinetic model with non-local sensing. arXiv preprint arXiv:190808325
- Makena MR, Rao R (2020) Subtype specific targeting of calcium signaling in breast cancer. *Cell Calcium* 85:102,109
- Meyer T, Stryer L (1988) Molecular model for receptor-stimulated calcium spiking. *Proc Natl Acad Sci Unit States Am* 85(14):5051–5055
- Monteith GR, McAndrew D, Faddy HM, Roberts-Thomson SJ (2007) Calcium and cancer: targeting  $\text{Ca}^{2+}$  transport. *Nat Rev Canc* 7(7):519
- Monteith GR, Prevarskaya N, Roberts-Thomson SJ (2017) The calcium–cancer signalling nexus. *Nat Rev Canc* 17(6):367
- Morales CP, Souza RF, Spechler SJ (2002) Hallmarks of cancer progression in barrett’s oesophagus. *The Lancet* 360(9345):1587–1589
- Morani F, Phadngam S, Follo C, Titone R, Thongrakard V, Galetto A, Alabiso O, Isidoro C (2014) Pten deficiency and mutant p53 confer glucose-addiction to thyroid cancer cells: impact of glucose depletion on cell proliferation, cell survival, autophagy and cell migration. *Genes Cancer* 5(7-8):226–39
- Murray JD (2003) *Mathematical Biology II: Spatial models and biomedical applications*
- Naik MU, Naik TU, Suckow AT, Duncan MK, Naik UP (2008) Attenuation of junctional adhesion molecule-a is a contributing factor for breast cancer cell invasion. *Cancer research* 68(7):2194–2203
- Narciso CE, Contento NM, Storey TJ, Hoelzle DJ, Zartman JJ (2017) Release of applied mechanical loading stimulates intercellular calcium waves in drosophila wing discs. *Biophysical journal* 113(2):491–501
- Painter K, Bloomfield J, Sherratt J, Gerisch A (2015) A nonlocal model for contact attraction and repulsion in heterogeneous cell populations. *Bull Math Biol* pp 1–34
- Palachanis D, Szabó A, Merks RM (2015) Particle-based simulation of ellipse-shaped particle aggregation as a model for vascular network formation. *Computational Particle Mechanics* 2(4):371–379
- Panetta JC, Chaplain MA, Cameron D (2000) Modelling the effects of paclitaxel and cisplatin on breast and ovarian cance. *Comp Math Meth Med* 3(1):11–23
- Panorchan P, Thompson MS, Davis KJ, Tseng Y, Konstantopoulos K, Wirtz D (2006) Single-molecule analysis of cadherin-mediated cell-cell adhesion. *Journal of cell science* 119(1):66–74
- Parekh AB (2011) Decoding cytosolic  $\text{Ca}^{2+}$  oscillations. *Trends in Biochemical Sciences* 36(2):78–87
- Politi A, Gaspers LD, Thomas J, Höfer T (2006) Models of  $\text{IP}_3$  and  $\text{Ca}^{2+}$  oscillations: frequency encoding and identification of underlying feedbacks. *Biophysical Journal* 90(9):3120–3133
- Powell J, Falcke M, Skupin A, Bellamy TC, Kypraios T, Thul R (2020) A Statistical View on Calcium Oscillations. *Advances in Experimental Medicine and Biology* 1131:799–826
- Prevarskaya N, Skryma R, Shuba Y (2013) Targeting  $\text{Ca}^{2+}$  transport in cancer: close reality or long perspective? *Expert opinion on therapeutic targets* 17(3):225–241
- Prevarskaya N, Ouadid-Ahidouch H, Skryma R, Shuba Y (2014) Remodelling of  $\text{Ca}^{2+}$  transport in cancer: how it contributes to cancer hallmarks? *Phil Trans R Soc B* 369(1638):20130,097
- Prevarskaya N, Skryma R, Shuba Y (2018) Ion channels in cancer: are cancer hallmarks oncochannelopathies? *Physiol Rev* 98(2):559–621
- Puck TT, Marcus PI, Cieciura SJ (1956) Clonal growth of mammalian cells in vitro: growth characteristics of colonies from single hela cells with and without a " feeder" layer. *Journal of Experimental Medicine* 103(2):273–284
- Ramis-Conde I, Drasdo D, Anderson AR, Chaplain MA (2008) Modeling the influence of the E-cadherin- $\beta$ -catenin pathway in cancer cell invasion: a multiscale approach. *Biophys J* 95(1):155–165
- Ramis-Conde I, Chaplain MA, Anderson AR, Drasdo D (2009) Multi-scale modelling of cancer cell intravasation: the role of cadherins in metastasis. *Phys Biol* 6(1):016,008

- Rezuchova I, Hudecova S, Soltysova A, Matuskova M, Durinikova E, Chovancova B, Zuzcak M, Cihova M, Burikova M, Penesova A, et al (2019) Type 3 inositol 1, 4, 5-trisphosphate receptor has antiapoptotic and proliferative role in cancer cells. *Cell Death & Disease* 10(3):186
- Roderick HL, Cook SJ (2008)  $\text{Ca}^{2+}$  signalling checkpoints in cancer: remodelling  $\text{Ca}^{2+}$  for cancer cell proliferation and survival. *Nat Rev Canc* 8(5):361
- Sanderson M, Sleight M (1981) Ciliary activity of cultured rabbit tracheal epithelium: beat pattern and metachrony. *Journal of cell science* 47(1):331–347
- Schuster S, Marhl M, Höfer T (2002) Modelling of simple and complex calcium oscillations. From single-cell responses to intercellular signalling. *European Journal of Biochemistry* 269(5):1333–1355
- Shapovalov G, Skryma R, Prevarskaya N (2013) Calcium channels and prostate cancer. *Recent Pat Anti-Canc* 8(1):18–26
- Shuai J, Pearson JE, Foskett JK, Mak DOD, Parker I (2007) A kinetic model of single and clustered  $\text{IP}_3$  receptors in the absence of  $\text{Ca}^{2+}$  feedback. *Biophysical Journal* 93(4):1151–1162
- Shuai JW, Jung P (2002) Stochastic properties of  $\text{Ca}^{2+}$  release of inositol 1,4,5-trisphosphate receptor clusters. *Biophysical Journal* 83(1):87–97
- Shuttleworth R, Trucu D (2019) Multiscale modelling of fibres dynamics and cell adhesion within moving boundary cancer invasion. *Bull Math Biol* pp 1–44
- Siekman I, Wagner LE, Yule D, Crampin EJ, Sneyd J (2012) A Kinetic Model for type I and II  $\text{IP}_3\text{R}$  accounting for mode changes. *Biophysical Journal* 103(4):658–668
- Simpson RU, Arnold AJ (1986) Calcium antagonizes 1, 25-dihydroxyvitamin D3 inhibition of breast cancer cell proliferation. *Endocrinology* 119(5):2284–2289
- Skupin A, Kettenmann H, Winkler U, Wartenberg M, Sauer H, Tovey SC, Taylor CW, Falcke M (2008) How does intracellular  $\text{Ca}^{2+}$  oscillate: by chance or by the clock? *Biophysical Journal* 94(6):2404–2411
- Slack-Davis JK, Atkins KA, Harrer C, Hershey ED, Conaway M (2009) Vascular cell adhesion molecule-1 is a regulator of ovarian cancer peritoneal metastasis. *Cancer research* 69(4):1469–1476
- Sneyd J, Dufour JF (2002) A dynamic model of the type-2 inositol trisphosphate receptor. *Proceedings of the National Academy of Sciences of the United States of America* 99(4):2398–2403
- Sneyd J, Falcke M (2005) Models of the inositol trisphosphate receptor. *Progress in Biophysics and Molecular Biology* 89(3):207–245
- Sneyd J, Han JM, Wang L, Chen J, Yang X, Tanimura A, Sanderson MJ, Kirk V, Yule DI (2017) On the dynamical structure of calcium oscillations. *Proceedings of the National Academy of Sciences of the United States of America* 114(7):1456–1461
- Sun CH, Wacquier B, Aguilar DI, Carayol N, Denis K, Boucherie S, Valencia Gallardo C, Simsek C, Erneux C, Lehman A, Enninga J, Arbibe L, Sansonetti P, Dupont G, Combettes L, Tran Van Nhieu G (2017) The *Shigella* type III effector IpgD recodes  $\text{Ca}^{2+}$  signals during invasion of epithelial cells. *EMBO Journal* 36(17):2567–2580
- Szymańska Z, Rodrigo CM, Lachowicz M, Chaplain MAJ (2009) Mathematical modelling of cancer invasion of tissue: the role and effect of nonlocal interactions. *Math Models Methods Appl Sci* 19(02):257–281
- Tang Y, Stephenson J, Othmer H (1996) Simplification and analysis of models of calcium dynamics based on  $\text{IP}_3$ -sensitive calcium channel kinetics. *Biophysical Journal* 70(1):246–263
- Taylor J, Simpson R (1992) Inhibition of cancer cell growth by calcium channel antagonists in the athymic mouse. *Cancer Res* 52(9):2413–2418
- Thul R (2014) Translating intracellular calcium signaling into models. *Cold Spring Harbor protocols* 2014(5)
- Thul R, Falcke M (2004a) Release currents of  $\text{IP}_3$  receptor channel clusters and concentration profiles. *Biophysical Journal* 86(5):2660–2673
- Thul R, Falcke M (2004b) Stability of membrane bound reactions. *Physical Review Letters* 93(18):188,103
- Thul R, Falcke M (2006) Frequency of elemental events of intracellular  $\text{Ca}^{2+}$  dynamics. *Physical Review E* 73(6 Pt 1):061,923

- Thul R, Falcke M (2007) Waiting time distributions for clusters of complex molecules. *Europhysics Letters* 79(3):38,003
- Thul R, Bellamy TC, Roderick HL, Bootman MD, Coombes S (2008) Calcium oscillations. *Advances in Experimental Medicine and Biology* 641:1–27
- Thul R, Thurley K, Falcke M (2009) Toward a predictive model of  $\text{Ca}^{2+}$  puffs. *Chaos* 19(3):037,108
- Thurley K, Smith IF, Tovey SC, Taylor CW, Parker I, Falcke M (2011) Timescales of  $\text{IP}_3$ -evoked  $\text{Ca}^{2+}$  spikes emerge from  $\text{Ca}^{2+}$  puffs only at the cellular level. *Biophysical Journal* 101(11):2638–2644
- Thurley K, Skupin A, Thul R, Falcke M (2012) Fundamental properties of  $\text{Ca}^{2+}$  signals. *Biochimica et Biophysica Acta* 1820(8):1185–1194
- Tilunaite A, Croft W, Russell N, Bellamy TC, Thul R (2017) A Bayesian approach to modelling heterogeneous calcium responses in cell populations. *PLoS Computational Biology* 13(10):e1005,794
- Tsaneva-Atanasova K, Yule DI, Sneyd J (2005) Calcium oscillations in a triplet of pancreatic acinar cells. *Biophysical Journal* 88(3):1535–1551
- Tsunoda T, Koga H, Yokomizo A, Tatsugami K, Eto M, Inokuchi J, Hirata A, Masuda K, Okumura K, Naito S (2005) Inositol 1,4,5-trisphosphate ( $\text{IP}_3$ ) receptor type 1 ( $\text{IP}_3\text{R1}$ ) modulates the acquisition of cisplatin resistance in bladder cancer cell lines. *Oncogene* 24(8):1396
- Uhlén P, Fritz N (2010) Biochemistry of calcium oscillations. *Biochemical and Biophysical Research Communications* 396(1):28–32
- Ullah G, Parker I, Mak DOD, Pearson JE (2012) Multi-scale data-driven modeling and observation of calcium puffs. *Cell Calcium* 52(2):152–160
- Virtanen P, Gommers R, Oliphant TE, Haberland M, Reddy T, Cournapeau D, Burovski E, Peterson P, Weckesser W, Bright J, et al (2019) Scipy 1.0—fundamental algorithms for scientific computing in python. arXiv e-prints p arXiv:1907.10121
- Voorsluijs V, Dawson SP, De Decker Y, Dupont G (2019) Deterministic Limit of Intracellular Calcium Spikes. *Physical Review Letters* 122(8):088,101
- Wang Z, Hillen T (2007) Pattern formation for a chemotaxis model with volume filling effects. *Chaos* 17(3):037,108
- Weinberg R (2013) *The biology of cancer*. Garland Science
- Weinberg SH, Smith GD (2014) The Influence of  $\text{Ca}^{2+}$  Buffers on Free  $[\text{Ca}^{2+}]$  Fluctuations and the Effective Volume of  $\text{Ca}^{2+}$  Microdomains. *Biophysical Journal* 106(12):2693–2709
- Weiner R, Schmitt B, Podhaisky H (1996) Rowmap—a row-code with krylov techniques for large stiff odes. report 39, fb mathematik und informatik universit at halle, germany
- Wieder N, Fink R, von Wegner F (2015) Exact Stochastic Simulation of a Calcium Microdomain Reveals the Impact of  $\text{Ca}^{2+}$  Fluctuations on  $\text{IP}_3\text{R}$  Gating. *Biophysj* 108(3):557–567
- Wijnhoven B, Dinjens W, Pignatelli M (2000) E-cadherin-catenin cell-cell adhesion complex and human cancer. *Br J Surg* 87(8):992–1005
- Wilkins M, Sneyd J (1998) Intercellular spiral waves of calcium. *J Theor Biol* 191(3):299–308
- Yang W, Chen JY, Zhou L (2009) Effects of shear stress on intracellular calcium change and histamine release in rat basophilic leukemia (RBL-2H3) cells. *Journal of Environmental Pathology, Toxicology and Oncology* 28(3)
- Young S, Ennes H, McRoberts J, Chaban V, Dea S, Mayer E (1999) Calcium waves in colonic myocytes produced by mechanical and receptor-mediated stimulation. *American Journal of Physiology-Gastrointestinal and Liver Physiology* 276(5):G1204–G1212
- Zhu D, Cheng CF, Pauli B (1992) Blocking of lung endothelial cell adhesion molecule-1 (Lu-ECAM-1) inhibits murine melanoma lung metastasis. *J Clin Invest* 89(6):1718–1724